https://doi.org/10.5194/egusphere-2026-3128
Preprint. Discussion started: 23 June 2026

Land-sea breeze contribution to pollutant dispersion from the Guinea Coastal cities of West Africa

E. Touré N'Datchoh[1,2], Peter Knippertz[2], Andreas H. Fink[2], Marlon Maranan[2], Julia Bruckert[2], Gholamali Hoshyaripour[2], Jasmin Haupt[2], and Arona Diedhiou[1,3]

[1]UFR SSMT, LASMES, University Félix Houphouët-Boigny Abidjan-Cocody, Abidjan, Côte d'Ivoire
[2]Institute of Meteorology and Climate Research Troposphere Research (IMKTRO), Karlsruhe Institute of Technology, Karlsruhe, Germany
[3]IRD; IGE - University Grenoble Alpes, Grenoble, France

Correspondence: E. T. N'Datchoh (ndatchoh.toure01@ufhb.edu.ci)

Abstract. Urbanization in Africa is often associated with increased air pollution, which affects not only the main cities but also remote regions depending on the prevailing meteorological conditions. Here, we investigate the role of the land-sea breeze (LSB) circulation for the dispersion of pollutants originating from five major coastal cities along the Guinea Coast in West Africa (Abidjan, Accra, Lomé, Cotonou, and Lagos). The study is based on a passive tracer emission experiment using the ICOsahedral Non-hydrostatic model coupled to the Aerosol and Reactive Trace gases module (ICON-ART) for a representative dry-season situation between 08 and 10 January 2021. Pollutants are emitted between 2 and 50 m from the ground from 0600 to 1800 UTC (close to local time) on the first day of simulation, from where they spread horizontally and vertically. The simulation reveals that the LSB starts to intensify near the coast around noon and propagates inland, reaching its maximum latitude at 7°N (approximately 200 km from the coasts) around 2100 UTC. Pollutants are first swiftly transported inland by the southwesterly wind of the LSB. As the planetary boundary layer deepens, particularly above the convergence zone near the LSB front, pollutants can reach the 875-800 hPa layer before being carried towards the coast and the Atlantic Ocean by the prevailing northeasterly return flow. Interestingly, these returning pollutants do not mix strongly down to the surface. Therefore, a well-developed LSB along the coast appears to contribute to attenuating urban coastal pollution by supporting a rapid dispersion of pollutants.

1 Introduction

Rapid urbanization in Africa has been associated with an increase in anthropogenic emissions (Keita et al., 2021; Wright et al., 2022). This is particularly true for West Africa, where the rapid growth of coastal cities such as Abidjan (Côte d'Ivoire), Dakar (Senegal), Lagos (Nigeria), Accra (Ghana) and Conakry (Guinea) has also led to widespread deforestation and changes in land use (Gnamien et al., 2024; Zhu et al., 2012). These emissions have an impact on local and regional air quality and climate, as was shown, for example, in the framework of the Dynamics-Aerosol-Chemistry-Cloud Interactions in West Africa (DACCIWA) project (Knippertz et al., 2015, 2017; Haslett et al., 2019; Adon et al., 2020; Djossou et al., 2018; Evans et al., 2018). These elevated levels of pollution are not only attributable to local sources, but also to long-range transport from other

https://doi.org/10.5194/egusphere-2026-3128
Preprint. Discussion started: 23 June 2026

parts of Africa. For the West African Monsoon (WAM) season in boreal summer, Flamant et al. (2018) found that aerosols in the lower troposphere are a mixture of emissions from coastal cities, such as Accra, Lomé, Cotonou and Lagos, with biomass burning aerosols from Central Africa and dust from the Sahara. During transport, the pollutant plumes from these coastal cities impact air quality over remote inland areas along their trajectories. Deroubaix et al. (2019) highlight high concentrations of pollutants near the surface between 1800 and 2200 UTC (1900 and 2300 local time) in Savè (Benin), almost 200 km north of Cotonou). Using the CHIMERE numerical model, they show that anthropogenic pollutants accumulated during the day near the coast are transported northward, once daytime convection in the planetary boundary layer (PBL) stops after 1600 UTC, and reach 8°N around 2100 UTC. Therefore, prevailing meteorological conditions play an important role in the dispersion of atmospheric pollutants.

The climate in the WAM region is determined by the annual shift of the intertropical discontinuity (ITD), which lies around 20°N in July (monsoon period) and around 8°N during January (dry season, (Fink et al., 2017)). The ITD separates the south-westerly winds that bring moisture from the Atlantic Ocean onto the continent from the north-easterly Harmattan winds that transport dust aerosols from the Sahel and Sahara regions (Engelstaedter et al., 2006; Touré et al., 2012) as well as aerosols from biomass burning in the Savannah regions from November to February (N'Datchoh et al., 2015). Well to the south of the ITD, there is a broad rainbelt that links with the intertropical convergence zone (ITCZ) over the ocean in the west. Across the Guinea Coast, almost throughout the year, low-level southwesterlies are dominant, reaching their peak at about 4 m s^{-1} during the WAM (Fink et al., 2017). In this period, nocturnal low-level jets (NLLJ) can form (Lothon et al., 2008; Abdou et al., 2010; Schrage and Fink, 2012; Schuster et al., 2013; Kalthoff et al., 2018) that carry pollution from the coastal belt inland (Knippertz et al., 2015). While the WAM season has been the focus of numerous studies and projects, the long dry season in the coastal region from November to the end of March has received less attention.

A wind regime limited to the immediate coastal region is the land-sea breeze (LSB; (Simpson, 1994)). The LSB system is defined as a local circulation related to the atmospheric temperature differences in the lower troposphere between the sea and the land surface. This atmospheric temperature contrast arises from the larger heat capacity of the ocean relative to land, which causes the atmosphere over land to warm (cool) more strongly than that over the ocean during daytime (nighttime) (Dragaud et al., 2019). Usually, the LSB starts during the morning, amplifies in the afternoon hours, and then ceases in the evening when the thermal gradient across the shore approaches zero. In the nighttime, an off-shore wind called the land breeze might develop (Miller et al., 2003). Guedje et al. (2019) investigated wind regimes over the Guinea Coastal region using surface and lower-tropospheric wind observations at Cotonou (Benin) and distinguished four wind regimes: Monsoon, Harmattan, NLLJ, and LSB. They highlight that all four wind regimes are important for the occurrence of coastal squall line systems and for the redistribution of pollutants emitted from coastal cities but without investigating the latter directly. Guedje et al. (2019) found that the lack of a diurnal reversal in wind direction obscured LSB activity at the peak of the southwesterly monsoon flow in boreal summer and during a period of stronger winds in March-April related to large land-sea thermal contrasts. During the WAM, the LSB increases due to background monsoon flow during daytime, while early morning land breeze occurrences were found to be infrequent in Cotonou (Guedje et al., 2019). In addition, early morning LSB in Cotonou appeared to peak during the main dry season in December, with a second peak occurring during the main rainy season in May–June. Over the coastal

https://doi.org/10.5194/egusphere-2026-3128
Preprint. Discussion started: 23 June 2026

region of Nigeria, LSB occurrences are most frequent from November to April and usually start as a light onshore near-surface wind a few hours after sunrise (Abayomi et al., 2007), while Parker et al. (2017) highlighted the prevalence of the LSB at Abidjan, Accra, and Cotonou during the dry season in January, when it contributes considerably to modulating temperatures by cooling the daytime maxima. Kouogang Tchuenkam et al. (2022) analysed LSB variability over the Cameroon coast in relation to the WAM. Interestingly, the LSB can show both clockwise and anti-clockwise hodograph rotations at the Guinea Coast (Coulibaly et al., 2019; Abayomi et al., 2007). Depending on the season, the convergence at the leading edge of the LSB front at the Guinea Coast can induce convective storms, sometimes even leading to flash flood events. The convection is often little organized but long-lasting during the afternoon and evening (Fink and Christoph, 2010) or merely generates shallow warm-rain showers in the deep monsoonal layer. The recent deforestation has led to an enhancement of the land-sea thermal contrast, which in turn has contributed to a doubling of the frequency of storms over the coastal deforested areas (Taylor et al., 2022).

The inland penetration of the LSB front usually varies between 10 km and 130 km (Miller et al., 2003). Recent work assessed the ability of the ICOsahedral Nonhydrostatic model (ICON) to reproduce the LSB over the Guinean coast of West Africa as well as the position of the sea breeze front, its propagation speed, and the height of the LSB density current (Haupt, 2024). The study found that a strong gradient in 10m wind speed and PBL height is clearly visible parallel to the coast and propagates inland, and that the sea breeze can transform into a NLLJ around 925 hPa after surface winds weaken. The work also showed that a few hours after sunset, when the atmosphere over land is cooled below the temperature of the atmosphere over the ocean, shallow weak offshore winds can emerge over land between the shoreline and a distance of 100 to 200 km inland. The question now arises how the LSB in connection with other wind systems affects horizontal and vertical pollutant transports and mixing. It is clear that low-level winds such as the LSB contribute to the dispersion of pollutants and air quality, but details will vary from region to region (Bouchlaghem et al., 2007; Varaprasad et al., 2024; de Coëtlogon et al., 2023; Shang et al., 2019; Crosman and Horel, 2010). There are indications for lifting of pollutants by the LSB front and a subsequent offshore transport with the return flow (Lawrence and Lelieveld, 2010), for pollutant concentrations near the coast, when the LSB interacts with other flows (Papanastasiou and Melas, 2009; Talbot et al., 2007), as well as for aerosols that are first transported out to sea and then brought back on land by the LSB (Crumeyrolle et al., 2019). The Guinea Coast is of particular interest because of emissions from its coastal megacities and from remote areas such as the Sahel-Sahara (Knippertz et al., 2017). For the WAM season Flamant et al. (2018) used numerical tracer release experiments to show that biomass burning emissions in Central Africa impact the surface aerosol and gaseous species concentrations in coastal cities such as Lagos (Nigeria) and Abidjan (Côte d'Ivoire). Depending on the altitude of the injection of these emissions, the pollutants follow different pathways: directly along the coast or over land toward the Sahel before being vertically mixed in the convective PBL and transported to the south-west and over the cities. Using the CHIMERE chemistry-transport model, de Coëtlogon et al. (2023) demonstrated that the impact on the inland transport of anthropogenic pollution depends on sea surface temperatures (SST) with warmer (colder) SSTs increasing (decreasing) the transport, especially during the night, suggesting an influence of the coastal upwelling intensity on the NLLJ. Until now, the transport of pollutants emitted along the Guinean coastal region during the dry season, is still poorly investigated and understood. Therefore, with the purpose of filling some existing gaps, this work aims to investigate the

https://doi.org/10.5194/egusphere-2026-3128
Preprint. Discussion started: 23 June 2026

pollutants dispersion by the LSB over the Guinean Coastal region during the dry season, using the ICON model coupled to the Aerosol and Reactive Trace gases (ART) module (ICON-ART).

2 Data and methods

The study domain for this work is southern West Africa, from 3°S to 13°N and from 12°W to 12°E, as shown in Figure 1. This domain spans from Nigeria to the Guinean Highlands in the east-west direction and from the Gabonese Coast to the Sahel in the south-north direction. This wide domain has been chosen to cover the entire Gulf of Guinea and enough land to understand the LSB and pollutant transport into the continent. In the following, we will provide information on the observational data used and the setup of the model.

2.1 Data

In this study, a number of different observational datasets are used for model validation. This includes station data, satellite products, and re-analysis data as detailed in the following.

2.1.1 TAHMO data

The Trans-African Hydro-Meteorological Observatory (TAHMO) is a project aiming to develop a dense network of hydrometeorological monitoring stations in sub-Saharan Africa – one every 30 km. Up to 20,000 stations are planned to be installed across the African continent. The TAHMO weather station technology is based on the ATMOS 41 model manufactured by the METER Group (https://www.metergroup.com/en/meter-environment/products/atmos-41-weather-station) and includes sensors to measure rainfall, temperature, atmospheric pressure, relative humidity, solar radiation, wind speed, and wind direction measurements. TAHMO stations have a 5-min measurement interval of meteorological variables (Dezfuli et al., 2017). In the study region, Kniffka et al. (2020) used TAHMO radiation data in southwestern Ghana to validate satellite surface solar radiation estimates. Furthermore, using TAHMO data in Burkina Faso for the period from May 2017 to December 2020, Schunke et al. (2021), for example, highlighted the potential opportunity and cost-efficient solution that TAHMO offers for hydrometeorological applications. TAHMO data are available at https://tahmo.org/?station=TA00675&variable=pr&period=H. For this study, 17 TAHMO stations (purple points and numbers in Figure 1) located in the coastal region of southern West Africa were used.

2.1.2 METAR

Meteorological Aerodrome Report (METAR) is a coded format for reporting weather information, available at a 30min time interval. It is described as the aerodrome routine meteorological report of the World Meteorological Organization (WMO). METAR messages are provided in real-time at a given airport (ICAO, 2010; WMO). These reports are issued primarily for flight planning and aviation safety. In general, METAR meteorological information is automatically measured by instruments and sensors located in the aerodromes. However, a human observer is also present to monitor the weather, adjusting and

https://doi.org/10.5194/egusphere-2026-3128
Preprint. Discussion started: 23 June 2026

completing the METAR when needed. Here, METAR data are used only for the Abidjan Airport Station (DIAP code for Abidjan Airport in the ICAO (International Civil Aviation Organization) database where reports are available together with a corresponding TAHMO station.

2.1.3 ECMWF operational analysis data

The ECMWF operational analysis with a spatial horizontal resolution of 9 km and 137 vertical levels is available at synoptic hours (0000, 0600, 1200, and 1800 UTC). These have been used widely for studies over tropical Africa (Vogel et al., 2020). ECWMF operational analysis, sea surface temperature (SST) are from the Operational Sea Surface Temperature and Ice Analysis (OSTIA). The ECMWF operational analysis in this work was interpolated onto the ICON-ART output horizontal grid resolution to facilitate comparison between the two datasets.

2.1.4 IMERG

IMERG (Integrated MultisatellitE Retrievals from Global Precipitation Measurement (GPM)) is a precipitation dataset with 0.1° spatial and 30 min temporal resolution (Huffman et al., 2018). IMERG combines precipitation retrievals from all available low-orbit passive microwave (PMW) data, together with geosynchronous infrared (GEO-IR) to compute merged global precipitation. The raw data are processed by the GPROF2017 algorithm (Kummerow, 2017) and then gridded and merged with the IR data to provide global homogeneous precipitation measurements. IMERG has three types of products, early (IMERG-E), late (IMERG-L), and final (IMERG-F). “early” and “late” products are available in quasi-near-real-time, and their final version is released 2.5 months later. An advantage of IMERG-F is that it includes additional satellite and calibration with surface rain-gauge stations data that may be delayed for any reason. The gridded data are available from 1998 to the present. Maranan et al. (2020) have shown that GPM IMERG has issues in detecting warm rains, which can occur on the LSB front. Here, IMERG-F data were used in the case study selection process.

2.2 ICON-ART model and passive tracers

The ICON-ART model is used to study the dispersion of pollutants from the coast of West Africa during LSB occurrence. ICON is a global atmospheric model that solves the full three-dimensional non-hydrostatic and compressible Navier-Stokes equations on a horizontally unstructured icosahedral grid (Zängl et al., 2015). Performing bisections of the grid triangles offers an intuitive way of grid refinement. ICON simulations can be performed on the global scale as well as on regional scale and allow one-way and two-way nesting in regions of interest down to horizontal grid mesh sizes on the order of a few hundreds of meters. ICON provides physical parameterization packages for numerical weather prediction, climate modeling, and large-eddy simulations (Zängl et al., 2015; Dipankar et al., 2015; Heinze et al., 2017). ICON has been used in the West African region during the DACCIWA project (Deetz et al., 2018; Kniffka et al., 2020).

The ART submodule extends ICON by the emission and transport of aerosols and trace gases, as well as aerosol dynamics, gas-phase chemistry and interactions with radiation and clouds (Rieger et al., 2015; Weimer et al., 2017; Schröter et al., 2018;

https://doi.org/10.5194/egusphere-2026-3128
Preprint. Discussion started: 23 June 2026

Hoshyaripour et al., 2026). In this study, we focus on the transport of pollutants described for the sake of simplicity using passive tracers, which in ART are only transported by advection and turbulence, but no interaction with other tracers or the surface is considered. This implies that passive tracers have an infinite lifetime (Schröter et al., 2018).

2.3 Case study selection and experimental set-up

This work focuses on the occurrence of a non-rainy LSB circulation at the Guinea Coast during the dry season. Parker et al. (2017) showed that the LSB over the Guinean Coast is often accompanied by a band of clouds parallels to the coast, which intensifies and moves inland between 1200 and 1800 UTC. The selection of a good case to study here was made in the following way: (1) Check manually for evidence of LSB occurrence using the Moderate Resolution Imaging Spectroradiometer (MODIS) satellite cloud image (TERRA and AQUA; see https://worldview.earthdata.nasa.gov/.; Figure 2 shows an example for the case of 08 January 2021 (09 and 10 January are available in the supplementary material Figure A1). (2) Check for rainfall occurrence using both TAHMO and IMERG data over the Guinea Coast and for the various stations shown in Figure 1. Days with rain were not selected. This simple subjective methodology enabled the selection of the case study of LSB occurrence during a 3-day period from 08 to 10 January 2021 for further investigation.

Figure 3 shows the wind arrow and temperature at 2m for the TAHMO stations at 0600 UTC, 0900 UTC, 1200 UTC, 1500 UTC, 1800 UTC and 2100 UTC on 08 January 2021 (09 and 10 January are shown in the supplementary material Figure A2). Most of these stations show a shift to a stronger wind blowing from the sea as the sun heats and the temperature rises, indicating the occurrence of the LSB.

Simulations were performed using two nested domains at 13 km (Figure 1) and 6 km spatial resolution during 07 to 10 January 2021. The first day (07 January) of the simulation was considered a spin-up and was not analyzed. The simulation domains were centered on 2° W and 5° N and 0°W and 6° N for the resolution of the domains at 13 km and 6 km with 70 vertical levels (surface level spanned from 42 to 70 with 29 levels for better capturing the LSB flow). The simulation configurations are similar to those suggested by the DWD for tropical regions and are found in Prill et al. (2022). Passive tracers from predefined sources in this study were located within the five main cities along the Guinean Coast (Figure 1), i.e. Abidjan (lon: 4.01° W, lat: 5.30° N), Accra (lon: 0.2° W, lat: 5.55° N), Lomé (lon: 1.21° E, lat: 6.12° N), Cotonou (lon: 2.42° E, lat: 6.36° N) and Lagos (lon: 3.39° E, lat: 6.45° N). The sources were set to emit from 0600 UTC to 1800 UTC at a height above ground between 2 and 50 m on 08 January 2021. After 1800 UTC on 08 January, passive tracer emission was stopped, allowing investigation of the transport mechanism by LSB. These point sources are to mimic anthropogenic urban sources with a strong diurnal cycle. A sensitivity test with nighttime emissions of passive tracers between 2100 and 0600 UTC was also carried out. The finer grid spacing in the nested domain of 6 km did not result in significant differences (less than 10 % differences for variables such as 2m temperature, dew point, surface pressure; see supplementary material Figure A3). As this nested domain did not capture the full pattern of pollutant transport, we decided to show only the 13-km results in the following sections.

https://doi.org/10.5194/egusphere-2026-3128
Preprint. Discussion started: 23 June 2026

3 Results

The following sections provide an assessment of ICON-ART model performance over the study area (section 3.1) and its ability to reproduce the LSB occurrence (section 3.2). Also, pollutant dispersion mechanisms during LSB occurrence are described (section 3.3). Then, the impacts of LSB occurrence on pollutants dispersion is discussed (section 3.4).

3.1 Assessment of ICON-ART performance

The performance of ICON-ART in simulating meteorological parameters is assessed using the ECMWF operational analysis, the 17 TAHMO stations (TAHMO) and Abidjan airport (METAR). Figure 4 shows a comparison of the spatial distribution of temperature at 2m and wind at 10m during the synoptic hours 0000, 0600, 1200 and 1800 UTC averaged over 08-10 January 2021.

For 0000 UTC, the ECMWF data (Figure 4a) show relatively weak temperature contrasts across the region with moderately strong southerly to southwesterly wind over the ocean and generally lower wind speeds over land. To the north of 9° N north-easterly winds prevails, indicating the typical ITD position during the dry season in the region. Warmest surface temperatures around 29° C are found over northern Ghana, while high orography regions (Cameroon highlands, Jos Plateau in Nigeria, Guinea highlands) show temperatures as low as 22° C. Figure 4b shows the corresponding plot for ICON-ART (but with a higher grid spacing) and Figure 4c the difference between the two. They reveal that ICON-ART has systematically higher temperatures (1-2° C) to the south of the Guinea Coast, while temperatures to the south of the equator are even slightly cooler. Over the continent, a mixture of cold and warm biases is observed. Overall, the ECMWF operational analysis tends to be warmer with a maximum of up to 4 ° C) between northern Benin and north-eastern Nigeria. This is to some extent related to a lower model topography given the coarser resolution of the ECMWF data, but this difference also occurs away from mountains, as in the coastal plains of Togo, Benin and Nigeria. Further to the west, from western Ghana to Liberia, ICON-ART tends to be warmer. Wind differences are rather unsystematic, but some more coherent features can be seen in the vicinity of large temperature differences, underlining the connection between temperature, pressure, and wind.

At 0600 UTC (Figure 4d), ECMWF data show the effect of nighttime cooling with minimum temperatures reaching 16° C over high terrain. Cooling is generally more pronounced in the drier north, where the smaller column water vapor allows more longwave radiation to escape to space. As expected, changes in temperature between 0000 and 0600 UTC are small over the ocean. The winds turn slightly more westerly over the Bight of Benin, with winds over land further slowing down in the stable nighttime PBL. ICON-ART (Figure 4e) shows a largely similar tendency such that the differences to ECMWF (Figure 4f) stay quite robust between 0000 and 0600 UTC. It is remarkable that the differences in wind over the ocean increase, with a somewhat stronger onshore flow in ICON-ART.

After sunrise, the continent warms up very quickly in the ECMWF operational analysis, reaching temperatures above 30° C from northwestern Nigeria to southern Mali at 1200 UTC (Figure 4g). While winds change little over the ocean, winds over southern West Africa become very weak and turn to easterlies over the Sahel. The corresponding plot for ICON-ART (Figure 4h) shows a similar warming pattern, reducing differences overall with a noisier spatial pattern (Figure 4i). Interestingly, ICON-

https://doi.org/10.5194/egusphere-2026-3128
Preprint. Discussion started: 23 June 2026

ART produces a much clearer inland flow over southern West Africa than ECMWF, leading to larger wind differences over land than over the ocean.

Finally in late afternoon, as the sun sets over the study area, temperatures begin to decrease again in the ECMWF analysis (Figure 4j), in particular in a coastal strip with onshore flow, while elsewhere on land winds tend to be fairly weak. Temperatures in ICON-ART (Figure 4k) have already fallen further leading to a positive difference over most land areas (Figure 4l). It is noteworthy that the onshore flow over the Bight of Benin is stronger in ECMWF data but then weaker over the immediate coastal zone. This suggests that ICON-ART may generate a stronger LSB despite the warmer temperatures in ECMWF.

To first order there is a good agreement between the operational ECMWF analysis and ICON-ART in capturing the main features in low-level temperature and wind over West Africa. It is somewhat surprising that there is a persistent warm bias in ICON-ART over the ocean, implying a smaller temperature contrast to the land during the day. Over land, ECMWF is overall warmer with some regional differences and a maximum at 1800 UTC. One reason is the somewhat lower topography in the coarser-resolution Integrated Forecasting System (IFS model), other potential reasons are differences in PBL dynamics, soil moisture or low cloud that affect radiation.

Though, in the present study, no radiosonde data were available for all the studied stations considered here, Kniffka et al. (2020) while using radiosondes, found that in general, difference between radiosonde data and ECMWF analysis are larger at 0000 and 0600 UTC, while strong daytime turbulent mixing in the PBL homogenizes the lower atmosphere, creating smaller differences at 1200 and 1800 UTC.

Figure 5 presents time-series of hourly T2m, surface pressure, dew point temperature, and wind speed at 10m for the station of Abidjan (Cote d'Ivoire) using ICON-ART, the ECMWF operational analysis, METAR and TAHMO. The ECMWF operational analysis at 9km and ICON-ART simulations at 13 km spatial resolution were extracted using the nearest point method and compared with available ground-based observations (TAHMO and METAR for Abidjan only). Since the wind speed of TAHMO was recorded at 2m and there is not enough information about the vertical stability, extrapolation to 10m using a wind profile approach has not been applied. The time-series for the remaining TAHMO stations as shown in Figure 5 is provided in Annex A4. In Figure 5, it can be seen that the diurnal cycle for the temperature (Figure 5a) and surface pressure (Figure 5c) of the Abidjan station is quite well reproduced. The relative lower amplitude of the temperature over the Abidjan station compared to TAHMO may be related to the fact that this station pixel in both ICON and ECMWF analysis is a mixture of land and ocean. Inland stations generally exhibit less amplitude difference (supplementary material Figure A4). ICON-ART exhibits generally lower surface pressure, which is explained by the representation of the coastline and interpolation effects between grids. The Abidjan station is located in a flat coastal region with complex land–sea transitions. Although the ICON-ART 10m wind speed pattern is better in agreement with the METAR wind pattern, on January 10 and 11, its amplitude is much lower (Figure 5d).

Pearson correlation coefficients for hourly values of the same quantities for the 3 days of the case study, are presented in Figure 6. Concerning the temperature at 2m and surface pressure, strong positive (> 0.75) correlation coefficients and significance (p-value <0.01) are found for most of the stations with the dataset used here. This indicates that ICON-ART quite well reproduces the diurnal cycle of the 2m temperature and surface pressure over these stations, despite some underesti-

https://doi.org/10.5194/egusphere-2026-3128
Preprint. Discussion started: 23 June 2026

mation/overestimation in their magnitude. However, the correlation coefficients for dew point temperatures show different patterns. A range of values from anti-correlation, no correlation, and strong correlation can be observed depending on the station and dataset considered. This points to issues in the models to represent details in moisture transport and vertical mixing in this complex coastal zone. It is worth noting that ICON-ART has been initiated on 07 January with one day used as spin-up; therefore, the low correlation values with the dew temperature are not related to spin-up. The Pearson correlation coefficient, for the wind speed at 10 m, could not be assessed due to the lack of information on vertical turbulence and caution with the quality of TAHMO wind speed measurements was reported by (Schunke et al., 2021).

3.2 LSB simulated with ICON-ART

Before using ICON-ART to investigate the role of LSB in pollutant dispersion, it is necessary to ensure that the LSB is well reproduced. LSB is known to develop and propagate under a local pressure gradient force directed towards the land due to the difference in atmospheric temperature between the land and the ocean, which induces a shallow movement of marine air toward the continent. The temperature and low-level gradients from the ocean to land at different times of the day during the case study were analyzed. Temperature gradients and wind arrows at 10 m (Figure 7) and absolute values of low-level wind gradients (Figure 8) as suggested by Haupt (2024) are used to illustrate LSB occurrence and its progression inland (cases of 09 and 10 January are shown in supplementary material Figures A5 and A6). At morning hours (0900 UTC, Figures 7a and 8a), north-easterly trade winds known as Harmattan dominate the northern portion of the study domain. At the same time, southwesterly monsoon winds can be observed over the southern portion, associated with a moderate temperature gradient and a maximum observed over the highland portion of Cameroon and the Jos Plateau in Nigeria, coinciding with the lower temperature over these highlands. As the sun warms the continent, the PBL deepens and surface winds weaken over both the ocean and land; moderate temperature and wind speed gradients can be observed (Figures 7b and 8b). This weakening of the near-surface southwesterly monsoon winds (1000 hPa and 925 hPa), is also evident in hourly vertical profiles of meridional and zonal wind) across the study domain between 2° S and 10 ° N and 12 ° W and 8 ° E (Figures A7 and A8). The zone of weak winds develops as sunshine increases (from 0900 UTC) and reaches its smallest spatial extent (around 1500 UTC) when the wind gradient strengthens, indicating the sea breeze development (Figure 7). The maximum temperature gradient of about 2° C/13 km spreads from southern Mali - Guinea in the west to central Nigeria in the east (Figure 7b). In the afternoon, around 1500 UTC (Figure 7c), when the land surface reaches its maximum temperature, the gradient is close to zero and a bluish band, expressing a positive temperature gradient (about 0.5° C/13 km), starts to develop along the Guinea Coast (from Nigeria to Côte d'Ivoire), as the wind speed simultaneously increases surrounding the bluish band (Figures 7c and 8c). Around 1800 UTC, the temperature gradient (Figure 7d) has increased in the band, while its progression further inland (around 6° N) is observed and a well-marked feature in the low-level wind speed gradient (Figure 8d). These patterns of temperature at 2m and low-levels wind speed gradients are located further over land (around 7° N) around 2100 UTC (Figures 7e and 8e) and (9° N) around 0000 UTC (Figures 7f and 8f). From its start along the coast (5° N in the early hours of the afternoon (around 1200 UTC) to its northward position (7° N, in the evening around 2100 UTC) the horizontal propagation of the LSB is about 2° (approximately 200 km in 6 hours). In Figure 9, the 2m temperature (a and b) and pressure gradients between (c-d) a

https://doi.org/10.5194/egusphere-2026-3128
Preprint. Discussion started: 23 June 2026

south-north line at Abidjan (3.93° W; 5.26° N) perpendicular to the coast with the southernmost point over the Gulf of Guinea at 50 km offshore and inland points at a distance of, respectively, 50 km, 100 km, and 150 km are presented for 08 January and both the ICON model simulation (9a and 9c) and the ECMWF operational analysis (Figure 9b and 9d). During the nighttime and until about 0900 UTC, the land surface remains cooler than the sea surface (Figure 9a-b). This configuration is unfavorable for the development of the sea breeze and rather corresponds to a land-breeze regime. Later in the morning hours, the thermal gradient becomes positive, indicating a rapid warming of the continent compare to the ocean. This thermal contrast generates a pressure gradient directed toward the land and thus favors the sea breeze establishment (Figure 9c-d). The temperature gradient reaches its maximum in the early afternoon, around 1300–1400 UTC for the ICON model (Figure 9a) and 1400–1500 UTC for ECMWF (Figure 9b). Well after sunrise (around 1000 UTC), incoming solar radiation heats the land surface more rapidly than the ocean surface.

This pattern promotes the establishment of a pressure gradient from the sea toward the land (Figure 9c-d). Although an overall similar diurnal cycle, ECMWF Operational Analysis tends to simulate slightly higher thermal gradients inland, particularly at 50 km and 100 km from the coast, suggesting a somewhat stronger sea-breeze circulation.

In conclusion, the ICON-ART simulations used here are able to reproduce the LSB occurrence with an inland propagation of up to 100-200 km, broadly consistent with previous literature (Miller et al., 2003; Haupt, 2024). We can now go on and investigate the implications for pollution dispersion.

3.3 ICON-ART tracer dispersion

3.3.1 Pollutant atmospheric column

Figure 10 illustrates the plume evolution of the passive tracer loaded within the atmospheric column together with wind vectors at 10m. As the pollutant source starts to emit at 0600 UTC, the pollutant plumes appear as small spots (Annex A5). The pollutant plume spots growth with time from 0600 to 1800 UTC (Figure 10a-i), and its northeastward transport toward further inland can be noticed. In addition, some small pollutant plumes can be seen over the Atlantic Ocean, with the maximum located around 6°N (Figure 10b). From 1800 UTC (Figure 10c), a rapid progression of the pollutant plume into the continent can be observed, with maximum values located around 7°N at 2100 UTC (Figure 10d), while the pollutant plume over the Atlantic Ocean has also expanded spatially. During the same time, the pollutant plume over the land expands and covers a wider area. At 0000 UTC on 09 January, the pollutant plume has passed 8 ° (Figure 10e). Overall, from 0000 UTC to 1200 UTC on 09 January (Figure 10f-i), pollutant plumes reach their northernmost position, passing 9° N. The remaining plume evolution is shown in the supplement material (Figure A9). Moreover, it is observed that the concentration of pollutants in the atmospheric column weakened during transport because of dilution with the surrounding air. The pollutants emitted are lifted upward as a result of PBL turbulence and upward motion. The 10 m wind thus cannot explain the observed spatial distribution pattern, as pollutants get redistributed beyond the 10m level. Overall, the pattern of the column plume transport matches the corresponding LSB features described in Section 3.2. However, the observed shape of pollutant plumes over the Atlantic Ocean cannot be explained by surface wind characteristics. Therefore, the vertical structure of pollutants and the associated wind needs to be

https://doi.org/10.5194/egusphere-2026-3128
Preprint. Discussion started: 23 June 2026

investigated to elucidate the mechanisms by which pollutant plumes reach the Atlantic Ocean despite the inland transport by the LSB.

3.3.2 Mechanism of pollutant dispersion by LSB

The evolution of the pollutant plume is now further investigated by analyzing individual horizontal layers at different stages of transport (Figure 11). As pollutant sources were confined between 2 and 50 m and set up to start emitting at 0600 UTC, when PBL turbulence is weak, pollutants are limited to the very low levels (between 1000 hPa and 975 hPa) over the land at 0700 UTC (Figure 11, first row). The vertical growth of the pollution layer appears to begin earlier in the east, where the sun rises earlier. As solar radiation increases and the land rapidly warms, there is an increase in turbulence within the PBL, mixing pollutants upward to reach 800 hPa (about 2000m) around 1200 UTC (Figure 11, second row), where a strong northeasterly flow prevails. However, at this time, the LSB is not yet well developed, and the pollution remains close to the coast.

When the LSB progresses inland during the afternoon, the pollution plumes stretch meridionally and reach about 200km inland at 1000 hPa by 1800 UTC (Figure 11, third row). Due to the stabilization of the PBL around sunset, the 925 hPa (Figure 11, third row, second column) layer is already tilted off from the sources immediately at the coast, in particular in the east, where the sun sets earlier. Interestingly, the 875 hPa level does not show such a clear separation from the coast, suggesting weaker inland transport above the LSB layer and possibly also downward mixing from the layer above, where north-easterlies prevail. At 800 hPa (Figure 11, third row, fourth column), pollutants have already clearly returned to the Atlantic Ocean.

Only three hours later, at 2100 UTC (Figure 11 - fourth row), pollutant plumes continue to progress northward, carried by the weakening LSB. At 925 hPa the separation of the plume from the coast has continued, while at 875 and 800 hPa (Figure 11 - fourth row, third and fourth columns) transports to the west and south further dilute the plume. Similar atmospheric conditions prevail at 0000 UTC (Figure 11 - fifth row), allowing the pollutant plume to continue progressing northward, while more pollutant reach 875 and 800 hPa, enhancing southeastward transport. At 0300 UTC, the plumes continue their inland progression at 1000 hPa, while pollutants get more diluted in the higher layers (925 -800 hPa) and finally reach the ITD (Figure 11 - sixth row), which is delimited by strong southwesterly winds prevailing at 925 hPa. At 0600 UTC, the head of the pollutant plume curves westward at 925hPa, allowing the Accra plume to reach the northern part of Togo and Ghana (Figure 11-seventh row), while pollutants continue their southwestward progression and more pollutants are transported over the Atlantic Ocean.

Thus, LSB occurrences during the dry season may favor pollution plumes emitted along cities of the Guinea Coast to move in a northeast direction, transported by low-level southwesterly winds. The plume observed over the Atlantic Ocean is due to strong northeasterly trade winds occurring at higher levels (Harmattan winds north of the ITD that rise above the air closer to the surface), creating a southwestward transport of the pollutant plume. Parker et al. (2017) reported that depending on atmospheric conditions, the vertical structure of the LSB can extend from 500 - 1000 m (lower layers) to 1000 - 2000 m (upper-level return flow). The backward transport of the pollutant plume to the sea above the landward cool flow behind the sea-breeze front was reported by Talbot et al. (2007) over the North Sea in Europe. However, here in the case of the Guinean coastal region, the transport of the pollutant plume backwards can be enhanced by the Harmattan northeasterly trade wind.

https://doi.org/10.5194/egusphere-2026-3128
Preprint. Discussion started: 23 June 2026

Despite only limited validation of ICON-ART wind fields with in-situ observations, the present results highlight the potential role that the LSB can play in pollutant transport in this coastal region.

Figure 12 summarizes the simulated plume evolution between 08 and 10 January 2021 from a meridional (Figure 12a-b), zonal (Figure 12c-d) and vertical (Figure 12e-f) perspective. The meridional perspective during the daytime case highlights the north- and southward transport patterns of the vertical average of the pollutant plume mass. Most of the pollutants preferentially travel in the northward direction. A southern branch of transport toward the Atlantic Ocean starts developing in the late afternoon hours and intensifies with time (Figure 12a). The zonal perspective during daytime emissions emphasizes the east- and westward transport (Figure 12c), with the eastward direction being the stronger one. A westward direction of transport also appears in the late afternoon/evening hours; this is more pronounced for the Abidjan plume transport. In the vertical profile columns of pollutants emitted from the five coastal cities during daytime, emissions propagate slowly toward the continent, while more and more pollutants accumulate in the simulation domain with time (Figure 12d). With the sun warming the land, the pollutant plumes spread toward the north, crossing 7° N around 1800 UTC while emissions between 1200 UTC and 1800 UTC accumulate. The plume is narrow during the morning hours before shifting to a broader eastward spread in the afternoon. Also, a westward transport of the pollutant can be observed for the Abidjan plume (Figure 12c). On vertical levels, pollutant plumes confined close to the surface initially increase sharply in the afternoon hours (Figure 12e), reaching beyond 700 hPa. This can be explained by processes such as convection and an increasing PBL depth associated with the progression of the LSB further inland, which mixes pollutants to higher altitudes. Between 1800 and 0000 UTC, pollutant plumes continue their progression inland, reaching 8° N, while smaller parts of the plume are diverted southward towards the Atlantic Ocean. Similarly, most of the plume spreads eastward but a fraction of it moves to the west. The vertical section reveals that pollutant plumes are confined between the surface and 900 hPa before being significantly reduced at the surface on the following day around 1200 UTC, as the LSB on 09 January starts to establish.

Pollutants emitted at nighttime remain longer in the surface layers and close to their source areas (Figure 12b, d and f). Transport to remote areas during nighttime is much slower than daytime, and the return flow of pollutants toward the Atlantic Ocean observed in the meridional section (Figure 12a) during daytime seems to be inhibited (Figure 12b). Also, the afternoon westward transport of the pollutant plume from Abidjan (Figure 12c), is less pronounced, and pollutants seem to be carried eastward (Figure 12d). Moreover, the pollutants appear to be rapidly lifted upward in vertical layers when the next-day LSB occurs (Figure 12f) compared to the daytime emission case (Figure 12e). This sensitive study highlights the importance of the role of the LSB in the dispersion of pollutants in West Africa. This behavior shows some similarity to the mechanism highlighted by Deroubaix et al. (2019), who found that anthropogenic pollutants from the coastal Guinean Gulf are transported within the PBL below 500 m above ground level during the WAM period.

Overall, the LSB occurrence during the dry season can support a rapid transport of pollutants from the coasts to remote inland areas with some of it returning to the coast with the northeasterly flow aloft. Outside the driest part of the season, the LSB occurrence may additionally contribute to the wet deposition of pollutants when the convergence at the leading edge triggers rainfall. However, deposition processes were not investigated here, as they are not included in the passive tracer experiment used here.

https://doi.org/10.5194/egusphere-2026-3128
Preprint. Discussion started: 23 June 2026

3.4 Implication for air pollution reduction in coastal urban areas

The cool sea breeze moves inland and regulates temperature around the coastal region and stabilizes the atmospheric profile, generally leading to clear skies (Parker et al., 2017). Therefore, these findings suggest that LSB occurrences at the Guinea Coast can contribute to lowering pollutant concentrations in coastal urban centers. Conversely, air quality in inland regions might be adversely affected, subject to local emission sources and atmospheric chemistry. It can be seen in Figure 11 that as the pollutant plumes travel inland transported by the LSB flow, their source points and surrounding areas become cleaner. Furthermore, LSB occurrences could potentially facilitate transport and dispersion of pollutant plumes toward regions to the north of coastal cities, which may, in turn, alleviate pollutant concentrations near their original sources as reported in previous work (Varaprasad et al., 2024; Jury and Buthelezi, 2022). The absence of LSB occurrence may cause the pollutants to remain longer around their source areas. The nighttime emission sensitivity revealed that the pollutants are transported over the source areas and slowly move in the northwestward direction. Thus, during a high pollution peak over the coastal cities of the Guinean Gulf, the occurrence of an LSB may favor rapid dispersion of the pollutant, contributing to clearing the coastal region. Furthermore, since the LSB has been reported to increase the frequency of afternoon showers at its leading edge, typically a few tens of kilometers (up to around 100 km) inland (Parker et al., 2017), it might contribute to a quick washout or rainout, if conditions are moist enough for rain generation. However, remote areas affected by pollutant plume transport (in the northeast ward direction of the coastal cities) will experience degradation of the air quality. Therefore, LSB occurrences on the Guinea Coast can contribute to reducing air pollution in coastal cities, while remote areas may experience poor air quality depending on the nature of pollutants and the chemical processes involved. Moreover, pollutant plumes have been found to be transported backward toward the Atlantic Ocean. This backward transport towards the Atlantic Ocean occurs in the atmospheric layers above about 800hPa, leaving the lower atmospheric levels crossed by this backward transport to be less impacted. Although the physical mechanisms involved in LSB may contribute to cleaning the lower atmospheric layers in the coastal region, it is worth noting that the current study did not investigate potential chemical processes that may occur due to LSB and the moisture brought along. As this study used passive tracers, chemical depletion, formation of aerosols from precursors, as well as interaction of secondary aerosols with clouds and radiation were not considered here. However, it was suggested by Augustin et al. (2020) that secondary aerosol formation may be enhanced due to the effect of both turbulence and temperature/humidity gradients between two contrasting air masses over the industrialized northern coastal region of France.

4 Conclusions

The dry season over the Guinean coastal region is still poorly investigated. Here, rapid population growth and urbanization, similar to many parts of sub-Saharan Africa, are causing air pollution to increasingly become an issue. Many details about sources are unknown and there is rather limited research on typical transport patterns in densely populated and thus strongly polluted areas. This work focuses specifically on the dispersion of pollutants by the LSB along the Guinea Coast during the dry season on the basis of a high-resolution passive tracer simulation using the ICON-ART model. The representative case study

https://doi.org/10.5194/egusphere-2026-3128
Preprint. Discussion started: 23 June 2026

chosen from 08 to 10 January 2021 was selected by inspecting MODIS satellite cloud imagery, IMERG and TAHMO surface station data over the Guinean coast.

The originality of this work consisted in focusing on the dry season, which has been less investigated so far. The ability of ICON-ART to reproduce the diurnal cycle of meteorological parameters during this season was assessed using ground-based measurements and gridded observations (operational analysis of ECMWF). Despite some biases, ICON-ART reproduces the main features reasonably well. Secondly, we examined the inland propagation of the LSB front using temperature and low-level wind gradients. During the dry season, the LSB starts developing in the early afternoon hours (1200 UTC) around 5°N and propagates inland, reaching its maximum position around 7°N (approximately 200 km from the coast) around 2100 UTC. The passive tracers emitted between 2 and 50 m in the coastal cities of Abidjan, Accra, Lomé, Cotonou, and Lagos were used to investigate the impact of LSB on the dispersal of pollutant in the region. Pollutants emitted from coastal cities during the dry season are primarily transported inland by the southwesterly flow behind the LSB front. This transport essentially takes place between the surface and 800 hPa. Moreover, backward transport of pollutants towards the Atlantic Ocean was highlighted. This backward transport takes place above the LSB layers, enhanced by a northeasterly wind prevailing between 875 hPa and 800 hPa (approximately 1200 and 2000 m above the surface). Sensitivity studies of nighttime coastal pollutant emissions revealed that pollutants will tend to accumulate longer in their source regions. Thus, it is plausible that LSB activity during the dry season contributes significantly to pollutant dispersion at the Guinea Coast. The return flow of the pollutant plume occurs with the Harmattan wind lifted above the air behind the LSB front. Therefore, the LSB occurrence during the dry season can contribute to attenuating urban coastal air pollution over the Guinean Coast, while inland remote areas downstream, on the contrary, may experience degradation of their air quality.

With the focus of this study on pollutant transport, the chemical composition and the potential for chemical or physical processing during transport were not taken into account, as was the contribution of maritime aerosols to local pollution. The same holds for removal processes. Future work will need to integrate these aspects to better understand air quality and possible impacts on human health in the region.

Data availability. The Trans-African Hydro-Meteorological Observatory (TAHMO) data can be retrieved from https://tahmo.org/. Interested parties may contact info@tahmo.org for these data.

Author contributions. Conceptualization and methodology, N.E.T., P.K. and A.H.F ; modeling experience, N.E.T, P.K, A.H.F, M.M, J.B, G.H and J.H writing—original draft preparation, N.E.T., P.K and A.H.F; writing—review and editing, N.E.T, P.K, A.H.F, M.M, J.B, G.H, J.H and A.D All authors have read and agreed to the published version of the manuscript.

Competing interests. At least one of the (co-)authors is a member of the editorial board of Atmospheric Chemistry and Physics

https://doi.org/10.5194/egusphere-2026-3128
Preprint. Discussion started: 23 June 2026

Acknowledgements. This work was supported by the Alexander von Humboldt Foundation under the Henriette Herz Scouting Program and the Karlsruhe Institute of Technology. The authors thank the Trans-African Hydrometeorological Observatory (TAHMO) for providing data from their station netowrk. This work was performed on the HoreKa supercomputer funded by the Ministry of Science, Research and the Arts Baden-Württemberg and by the Federal Ministry of Education and Research.

https://doi.org/10.5194/egusphere-2026-3128
Preprint. Discussion started: 23 June 2026

References

Abayomi, A., Abiodun, B., and Omotosho, B.: An observational study of sea breeze over Nigerian coastal region, Res, J. Appl. Sci, 2, 745–751, 2007.

Abdou, K., Parker, D. J., Brooks, B., Kalthoff, N., and Lebel, T.: The diurnal cycle of lower boundary-layer wind in the West African monsoon, Quarterly Journal of the Royal Meteorological Society, 136, 66–76, 2010.

Adon, A. J., Liousse, C., Doumbia, E. T., Baeza-Squiban, A., Cachier, H., Léon, J.-F., Yoboué, V., Akpo, A. B., Galy-Lacaux, C., Guinot, B., et al.: Physico-chemical characterization of urban aerosols from specific combustion sources in West Africa at Abidjan in Côte d'Ivoire and Cotonou in Benin in the frame of the DACCIWA program, Atmospheric Chemistry and Physics, 20, 5327–5354, 2020.

Augustin, P., Billet, S., Crumeyrolle, S., Deboudt, K., Dieudonné, E., Flament, P., Fourmentin, M., Guilbaud, S., Hanoune, B., Landkocz, Y., et al.: Impact of sea breeze dynamics on atmospheric pollutants and their toxicity in industrial and urban coastal environments, Remote Sensing, 12, 648, 2020.

Bouchlaghem, K., Mansour, F. B., and Elouragini, S.: Impact of a sea breeze event on air pollution at the Eastern Tunisian Coast, Atmospheric Research, 86, 162–172, 2007.

Coulibaly, A., Omotosho, B. J., Sylla, M. B., Coulibaly, A., and Ballo, A.: Characteristics of land and sea breezes along the Guinea Coast of West Africa, Theoretical and Applied Climatology, 138, 953–971, 2019.

Crosman, E. T. and Horel, J. D.: Sea and lake breezes: A review of numerical studies, Boundary-layer meteorology, 137, 1–29, 2010.

Crumeyrolle, S., Augustin, P., Rivellini, L.-H., Choël, M., Riffault, V., Deboudt, K., Fourmentin, M., Dieudonné, E., Delbarre, H., Derimian, Y., et al.: Aerosol variability induced by atmospheric dynamics in a coastal area of Senegal, North-Western Africa, Atmospheric Environment, 203, 228–241, 2019.

de Coëtlogon, G., Deroubaix, A., Flamant, C., Menut, L., and Gaetani, M.: Impact of the Guinea coast upwelling on atmospheric dynamics, precipitation and pollutant transport over southern West Africa, Atmospheric Chemistry and Physics, 23, 15 507–15 521, 2023.

Deetz, K., Vogel, H., Knippertz, P., Adler, B., Taylor, J., Coe, H., Bower, K., Haslett, S., Flynn, M., Dorsey, J., et al.: Numerical simulations of aerosol radiative effects and their impact on clouds and atmospheric dynamics over southern West Africa, Atmospheric Chemistry and Physics, 18, 9767–9788, 2018.

Deroubaix, A., Menut, L., Flamant, C., Brito, J., Denjean, C., Dreiling, V., Fink, A., Jambert, C., Kalthoff, N., Knippertz, P., et al.: Diurnal cycle of coastal anthropogenic pollutant transport over southern West Africa during the DACCIWA campaign, Atmospheric Chemistry and Physics, 19, 473–497, 2019.

Dezfuli, A. K., Ichoku, C. M., Huffman, G. J., Mohr, K. I., Selker, J. S., van de Giesen, N., Hochreutener, R., and Annor, F. O.: Validation of IMERG precipitation in Africa, Journal of Hydrometeorology, 18, 2817–2825, 2017.

Dipankar, A., Stevens, B., Heinze, R., Moseley, C., Zängl, G., Giorgetta, M., and Brdar, S.: Large eddy simulation using the general circulation model ICON, Journal of Advances in Modeling Earth Systems, 7, 963–986, 2015.

Djossou, J., Léon, J.-F., Akpo, A. B., Liousse, C., Yoboué, V., Bedou, M., Bodjrenou, M., Chiron, C., Galy-Lacaux, C., Gardrat, E., et al.: Mass concentration, optical depth and carbon composition of particulate matter in the major southern West African cities of Cotonou (Benin) and Abidjan (Côte d'Ivoire), Atmospheric Chemistry and Physics, 18, 6275–6291, 2018.

Dragaud, I. C. D. V., Soares da Silva, M., Assad, L. P. d. F., Cataldi, M., Landau, L., Elias, R. N., and Pimentel, L. C. G.: The impact of SST on the wind and air temperature simulations: a case study for the coastal region of the Rio de Janeiro state, Meteorology and Atmospheric Physics, 131, 1083–1097, 2019.

https://doi.org/10.5194/egusphere-2026-3128
Preprint. Discussion started: 23 June 2026

Engelstaedter, S., Tegen, I., and Washington, R.: North African dust emissions and transport, Earth-Science Reviews, 79, 73–100, 2006.

Evans, M., Knippertz, P., Akpo, A., Allan, R. P., Amekudzi, L., Brooks, B., Chiu, J. C., Coe, H., Fink, A. H., Flamant, C., et al.: Policy findings from the DACCIWA Project, 2018.

Fink, A. and Christoph, M.: Impacts of Global Change, Impacts of global change on the hydrological cycle in west and northwest Africa, pp. 12–28, 2010.

Fink, A. H., Engel, T., Ermert, V., Van Der Linden, R., Schneidewind, M., Redl, R., Afiesimama, E., Thiaw, W. M., Yorke, C., Evans, M., et al.: Mean climate and seasonal cycle, Meteorology of tropical West Africa: The forecasters' handbook, pp. 1–39, 2017.

Flamant, C., Deroubaix, A., Chazette, P., Brito, J., Gaetani, M., Knippertz, P., Fink, A. H., de Coetlogon, G., Menut, L., Colomb, A., et al.: Aerosol distribution in the northern Gulf of Guinea: local anthropogenic sources, long-range transport, and the role of coastal shallow circulations, Atmospheric Chemistry and Physics, 18, 12 363–12 389, 2018.

Gnamien, S., Liousse, C., Keita, S., Kumar, R., and Yoboué, V.: High-Resolution Modeling of Air Quality in Abidjan (Côte d'Ivoire) Using a New Urban-Scale Inventory, Atmosphere, 15, 758, 2024.

Guedje, F. K., Houeto, A. V., Houngninou, E. B., Fink, A. H., and Knippertz, P.: Climatology of coastal wind regimes in Benin, Meteorologische Zeitschrift, 28, 23, 2019.

Haslett, S. L., Taylor, J. W., Evans, M., Morris, E., Vogel, B., Dajuma, A., Brito, J., Batenburg, A. M., Borrmann, S., Schneider, J., et al.: Remote biomass burning dominates southern West African air pollution during the monsoon, Atmospheric Chemistry and Physics, 19, 15 217–15 234, 2019.

Haupt, J.: The Land-sea Breeze Along the Guinea Coast and Its Sensitivity to Sea-surface Temperature Variations, 2024.

Heinze, R., Dipankar, A., Henken, C. C., Moseley, C., Sourdeval, O., Trömel, S., Xie, X., Adamidis, P., Ament, F., Baars, H., et al.: Large-eddy simulations over Germany using ICON: A comprehensive evaluation, Quarterly Journal of the Royal Meteorological Society, 143, 69–100, 2017.

Hoshyaripour, G. A., Baer, A., Bierbauer, S., Bruckert, J., Brunner, D., Förstner, J., Hamzehloo, A., Hanft, V., Keller, C., Klose, M., Kumar, P., Ludwig, P., Metzner, E., Muth, L., Pauling, A., Porz, N., Ramezani Ziarani, M., Reddmann, T., Reißig, L., Ruhnke, R., Satitkovitchai, K., Seifert, A., Sinnhuber, M., Steiner, M., Versick, S., Vogel, H., Weimer, M., Werchner, S., and Hoose, C.: The atmospheric composition component of the ICON modeling framework: ICON-ART version 2025.10, Geoscientific Model Development, 19, 1645–1681, https://doi.org/10.5194/gmd-19-1645-2026, 2026.

Huffman, G. J., Bolvin, D. T., Braithwaite, D., Hsu, K., Joyce, R., Kidd, C., Nelkin, E. J., Sorooshian, S., Tan, J., and Xie, P.: NASA global precipitation measurement (GPM) integrated multi-satellite retrievals for GPM (IMERG), Algorithm Theoretical Basis Document (ATBD) Version, 4, 2018.

ICAO, A.: Meteorological service for international air navigation, 2010.

Jury, M. R. and Buthelezi, M. S.: Air Pollution Dispersion over Durban, South Africa, Atmosphere, 13, 811, 2022.

Kalthoff, N., Lohou, F., Brooks, B., Jegede, G., Adler, B., Babić, K., Dione, C., Ajao, A., Amekudzi, L. K., Aryee, J. N., et al.: An overview of the diurnal cycle of the atmospheric boundary layer during the West African monsoon season: results from the 2016 observational campaign, Atmospheric Chemistry and Physics, 18, 2913–2928, 2018.

Keita, S., Liousse, C., Assamoi, E.-M., Doumbia, T., N'Datchoh, E. T., Gnamien, S., Elguindi, N., Granier, C., and Yoboué, V.: African anthropogenic emissions inventory for gases and particles from 1990 to 2015, Earth System Science Data, 13, 3691–3705, 2021.

https://doi.org/10.5194/egusphere-2026-3128
Preprint. Discussion started: 23 June 2026

Kniffka, A., Knippertz, P., Fink, A. H., Benedetti, A., Brooks, M. E., Hill, P. G., Maranan, M., Pante, G., and Vogel, B.: An evaluation of operational and research weather forecasts for southern West Africa using observations from the DACCIWA field campaign in June–July 2016, Quarterly Journal of the Royal Meteorological Society, 146, 1121–1148, 2020.

Knippertz, P., Evans, M. J., Field, P. R., Fink, A. H., Liousse, C., and Marsham, J. H.: The possible role of local air pollution in climate change in West Africa, Nature Climate Change, 5, 815–822, 2015.

Knippertz, P., Fink, A. H., Deroubaix, A., Morris, E., Tocquer, F., Evans, M. J., Flamant, C., Gaetani, M., Lavaysse, C., Mari, C., et al.: A meteorological and chemical overview of the DACCIWA field campaign in West Africa in June–July 2016, Atmospheric Chemistry and Physics, 17, 10 893–10 918, 2017.

Kouogang Tchuenkam, F. C., Mama, A. C., Gah-Muti, S. Y., and Araujo, M.: Variability of Sea Breezes Over the Cameroonian Coast and Their Interaction With the West African Monsoon, Frontiers in Earth Science, 10, 848 684, 2022.

Kummerow, C.: GPROF2017 Version 1, NASA/GSFC: Greenbelt, MD, USA, 2017.

Lawrence, M. and Lelieveld, J.: Atmospheric pollutant outflow from southern Asia: a review, Atmospheric Chemistry and Physics, 10, 11 017–11 096, 2010.

Lothon, M., Saïd, F., Lohou, F., and Campistron, B.: Observation of the diurnal cycle in the low troposphere of West Africa, Monthly Weather Review, 136, 3477–3500, 2008.

Maranan, M., Fink, A. H., Knippertz, P., Amekudzi, L. K., Atiah, W. A., and Stengel, M.: A process-based validation of GPM IMERG and its sources using a mesoscale rain gauge network in the West African forest zone, Journal of Hydrometeorology, 21, 729–749, 2020.

Miller, S., Keim, B., Talbot, R., and Mao, H.: Sea breeze: Structure, forecasting, and impacts, Reviews of geophysics, 41, 2003.

N'Datchoh, E., Konaré, A., Diedhiou, A., Diawara, A., Quansah, E., and Assamoi, P.: Effects of climate variability on savannah fire regimes in West Africa, Earth System Dynamics, 6, 161–174, 2015.

Papanastasiou, D. and Melas, D.: Climatology and impact on air quality of sea breeze in an urban coastal environment, International Journal of Climatology: A Journal of the Royal Meteorological Society, 29, 305–315, 2009.

Parker, D. J., Kassimou, A., Orji, B. N., Osika, D. P., Hamza, I., Diop-Kane, M., Fink, A., Galvin, J., Guichard, F., Lamptey, B. L., et al.: Local weather, Meteorology of Tropical West Africa: The Forecasters' Handbook, pp. 130–174, 2017.

Prill, F., Reinert, D., Rieger, D., and Zängl, G.: ICON tutorial, Working with the ICON Model. Available online: https://www. dwd. de/DE/leistungen/nwv_icon_tutorial/pdf_einzelbaende/icon_tutorial2020. pdf, 2022.

Rieger, D., Bangert, M., Bischoff-Gauss, I., Förstner, J., Lundgren, K., Reinert, D., Schröter, J., Vogel, H., Zängl, G., Ruhnke, R., et al.: ICON-ART 1.0–a new online-coupled model system from the global to regional scale, Geoscientific Model Development Discussions, 8, 567–614, 2015.

Schrage, J. M. and Fink, A. H.: Nocturnal continental low-level stratus over tropical West Africa: Observations and possible mechanisms controlling its onset, Monthly Weather Review, 140, 1794–1809, 2012.

Schröter, J., Rieger, D., Stassen, C., Vogel, H., Weimer, M., Werchner, S., Förstner, J., Prill, F., Reinert, D., Zängl, G., et al.: ICON-ART 2.1: A flexible tracer framework and its application for composition studies in numerical weather forecasting and climate simulations, Geoscientific Model Development, 11, 4043–4068, 2018.

Schunke, J., Laux, P., Bliefernicht, J., Waongo, M., Sawadogo, W., and Kunstmann, H.: Exploring the potential of the cost-efficient TAHMO observation data for hydro-meteorological applications in Sub-Saharan Africa, Water, 13, 3308, 2021.

Schuster, R., Fink, A. H., and Knippertz, P.: Formation and maintenance of nocturnal low-level stratus over the southern West African monsoon region during AMMA 2006, Journal of the Atmospheric Sciences, 70, 2337–2355, 2013.

https://doi.org/10.5194/egusphere-2026-3128
Preprint. Discussion started: 23 June 2026

Shang, F., Chen, D., Guo, X., Lang, J., Zhou, Y., Li, Y., and Fu, X.: Impact of sea breeze circulation on the transport of ship emissions in Tangshan port, China, Atmosphere, 10, 723, 2019.

Simpson, J. E.: Sea breeze and local winds, cambridge university press, 1994.

Talbot, C., Augustin, P., Leroy, C., Willart, V., Delbarre, H., and Khomenko, G.: Impact of a sea breeze on the boundary-layer dynamics and the atmospheric stratification in a coastal area of the North Sea, Boundary-Layer Meteorology, 125, 133–154, 2007.

Taylor, C. M., Klein, C., Parker, D. J., Gerard, F., Semeena, V. S., Barton, E. J., and Harris, B. L.: "Late-stage" deforestation enhances storm trends in coastal West Africa, Proceedings of the National Academy of Sciences, 119, e2109285 119, 2022.

Touré, N. D. E., Konaré, A., and Silué, S.: Intercontinental transport and climatic impact of Saharan and Sahelian dust, Advances in Meteorology, 2012, 157 020, 2012.

Varaprasad, V., Kanawade, V., and Narayana, A.: Association between sea-land breeze and particulate matter in five coastal urban locations in India, Science of The Total Environment, 913, 169 773, 2024.

Vogel, P., Knippertz, P., Fink, A. H., Schlueter, A., and Gneiting, T.: Skill of global raw and postprocessed ensemble predictions of rainfall in the tropics, Weather and Forecasting, 35, 2367–2385, 2020.

Weimer, M., Schröter, J., Eckstein, J., Deetz, K., Neumaier, M., Fischbeck, G., Hu, L., Millet, D. B., Rieger, D., Vogel, H., et al.: An emission module for ICON-ART 2.0: implementation and simulations of acetone, Geoscientific Model Development, 10, 2471–2494, 2017.

WMO: Aerodrome reports and forecasts: a users' handbook to the codes, 782.

Wright, C., Alo, B., Garland, R., Chirinda, N., Kituyi, E., Khomsi, K., Tchuikoua, L. B., Ozor, N., Zakari, I. S., Liebenberg-Enslin, H., et al.: Integrated Assessment of Air Pollution and Climate Change for Sustainable Development in Africa-Summary for Decision Makers, Integrated Assessment of Air Pollution and Climate Change for Sustainable Development in Africa-Summary for Decision Makers, 2022.

Zängl, G., Reinert, D., Rípodas, P., and Baldauf, M.: The ICON (ICOsahedral Non-hydrostatic) modelling framework of DWD and MPI-M: Description of the non-hydrostatic dynamical core, Quarterly Journal of the Royal Meteorological Society, 141, 563–579, 2015.

Zhu, T., Melamed, M. L., Parrish, D., Gauss, M., Klenner, L. G., Lawrence, M. G., Konare, A., and Liousse, C.: WMO/IGAC impacts of megacities on air pollution and climate, 2012.

https://doi.org/10.5194/egusphere-2026-3128
Preprint. Discussion started: 23 June 2026

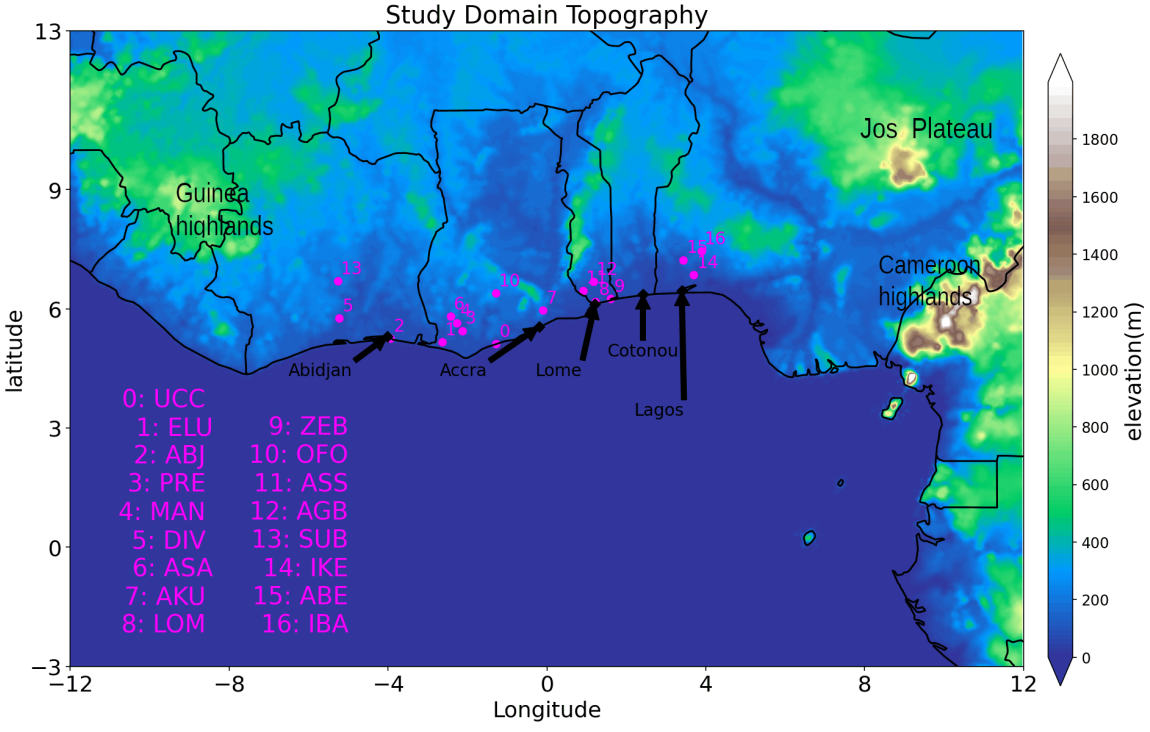

Figure 1. Topography of the study domain (shaded) based on ICON-ART with a grid spacing of 13 km. Purple points and numbers represent TAHMO stations as detailed in the list provided. Black diamonds represent the major city source points used for pollutant emissions in the tracers experiments.

https://doi.org/10.5194/egusphere-2026-3128
Preprint. Discussion started: 23 June 2026

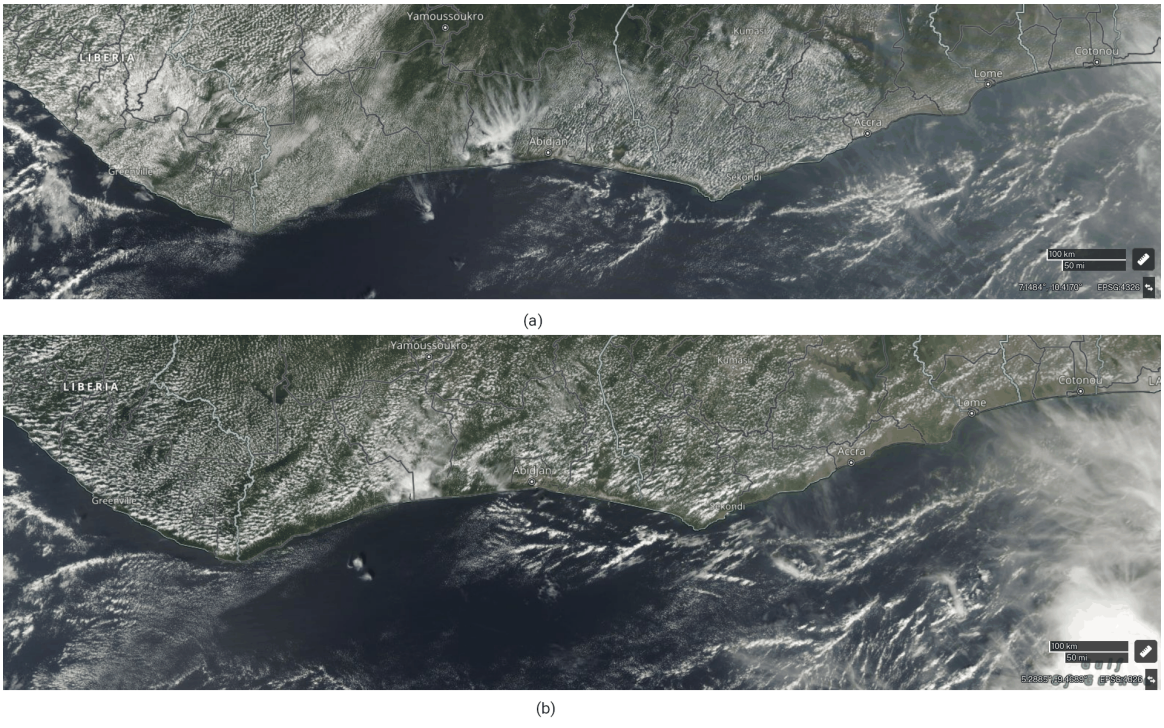

Figure 2. Observational evidence of the LSB occurrence from MODIS cloud cover (a) AQUA and (b) TERRA for the case study on 08 January 2021.

https://doi.org/10.5194/egusphere-2026-3128
Preprint. Discussion started: 23 June 2026

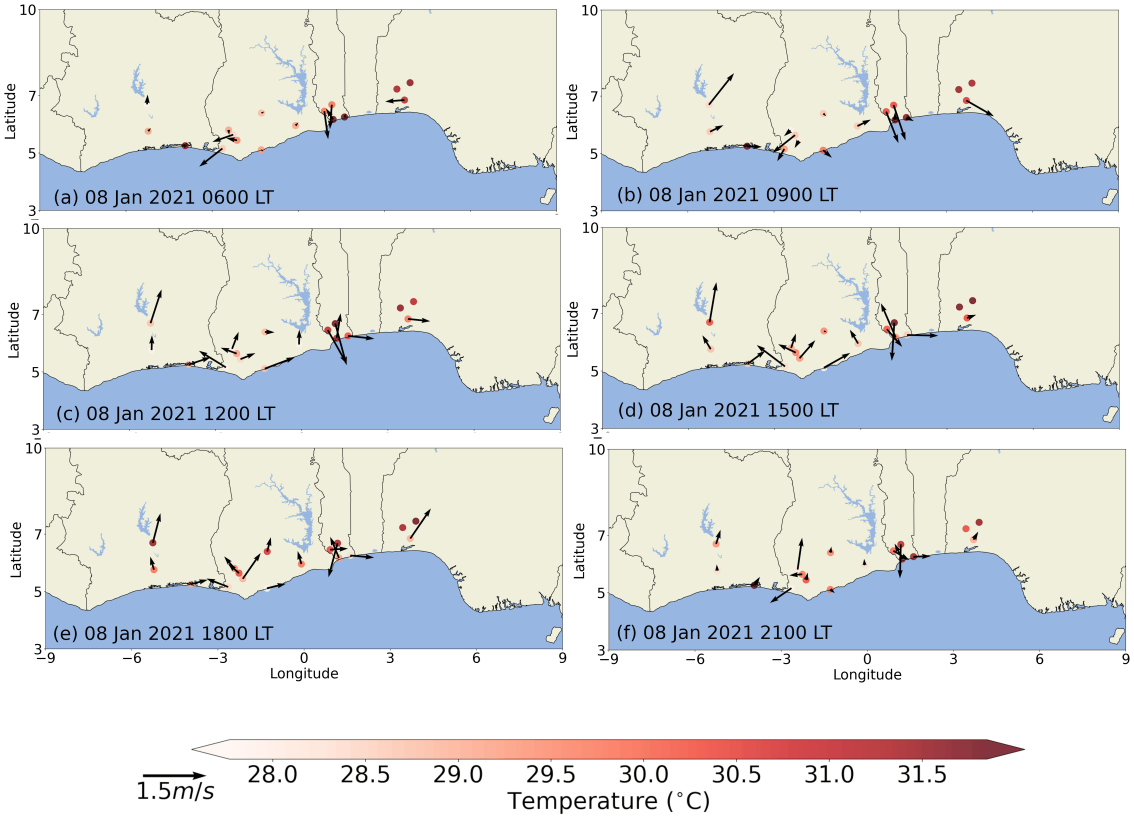

Figure 3. TAHMO stations showing wind at 2m (arrows) and temperature at 2m (shaded) at the synoptic hours (a) 0600, (b) 0900, (c) 1200, (d) 1500, (e) 1800 and (f) 2100 LT(UTC for stations located in Cote d'Ivoire, Ghana and Togo, and UTC+1 for station in Benin and Nigeria) on 08 January 2021.

https://doi.org/10.5194/egusphere-2026-3128
Preprint. Discussion started: 23 June 2026

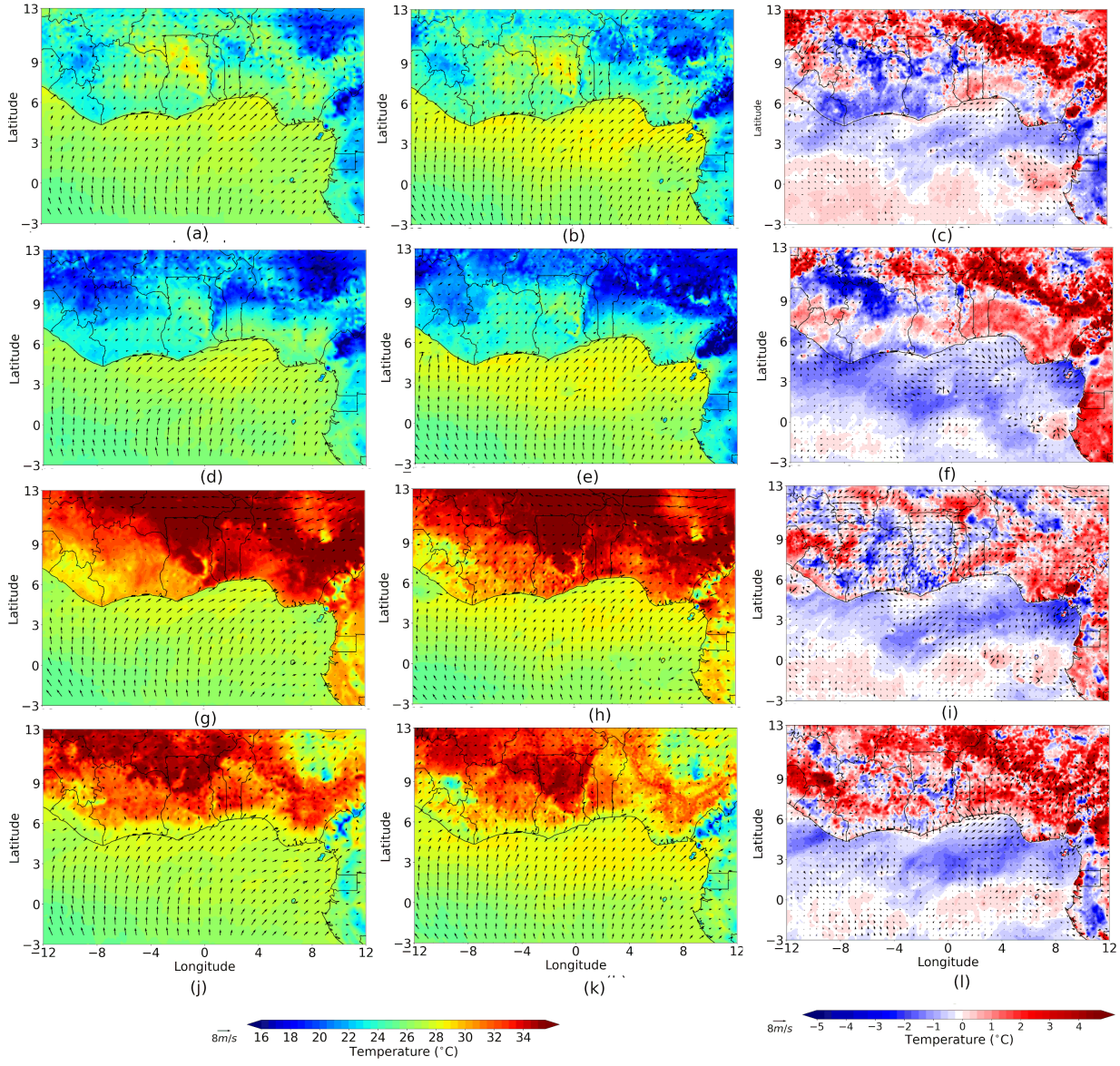

Figure 4. Three days-mean spatial distribution of 2m temperature (shaded) and 10m wind arrows from the ECMWF operational analysis (first column: a, d, g and j) and ICON-ART (second column: b, e, h and k) and their differences by interpolating ECMWF operational analysis on the ICON-ART grid (third column: c, f, i and l) between 08 and 10 January 2021 at the synoptic hours 0000, 0600, 1200 and 1800 UTC.

https://doi.org/10.5194/egusphere-2026-3128
Preprint. Discussion started: 23 June 2026

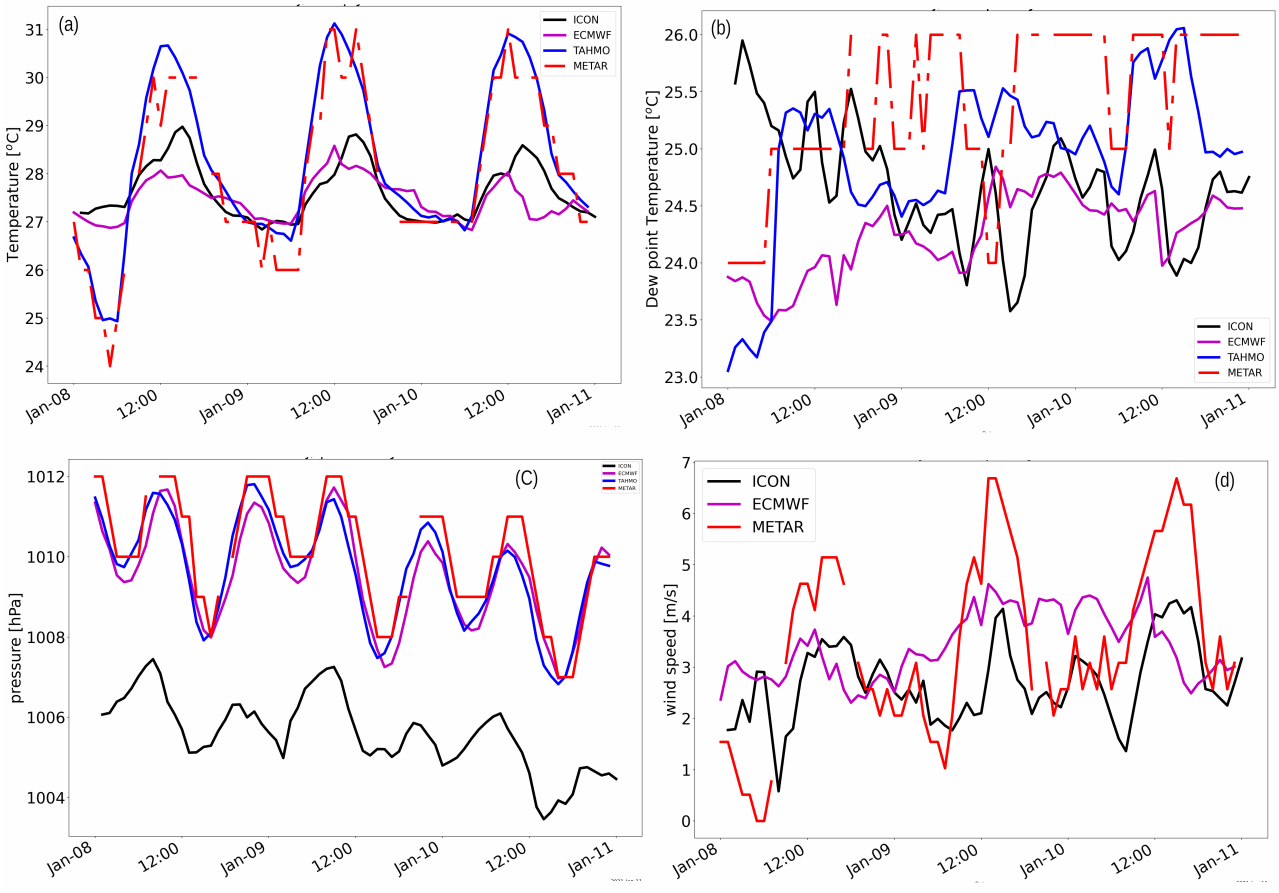

Figure 5. Hourly time series of (a) T2m, (b) dew point temperature at 2m, (c) surface pressure and (d) 10m wind speed at Abidjan station (3.93°W, 5.26°N) during 08 to 10 January 2021 from four different data sources (colors).

https://doi.org/10.5194/egusphere-2026-3128
Preprint. Discussion started: 23 June 2026

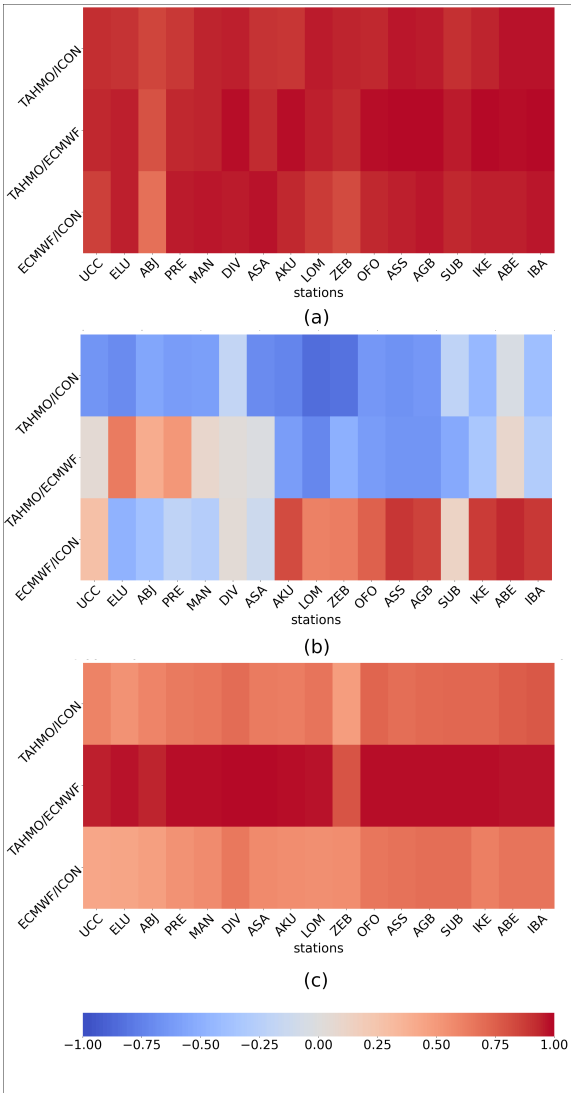

Figure 6. Significant (p-value <0.01) correlation coefficients between hourly values of (a) temperature at 2m, (b) dew point temperature at 2m and (c) and surface pressure for the 17 TAHMO stations as shown in Figure 1, ECMWF operational analysis during 08 to 10th January 2021

https://doi.org/10.5194/egusphere-2026-3128
Preprint. Discussion started: 23 June 2026

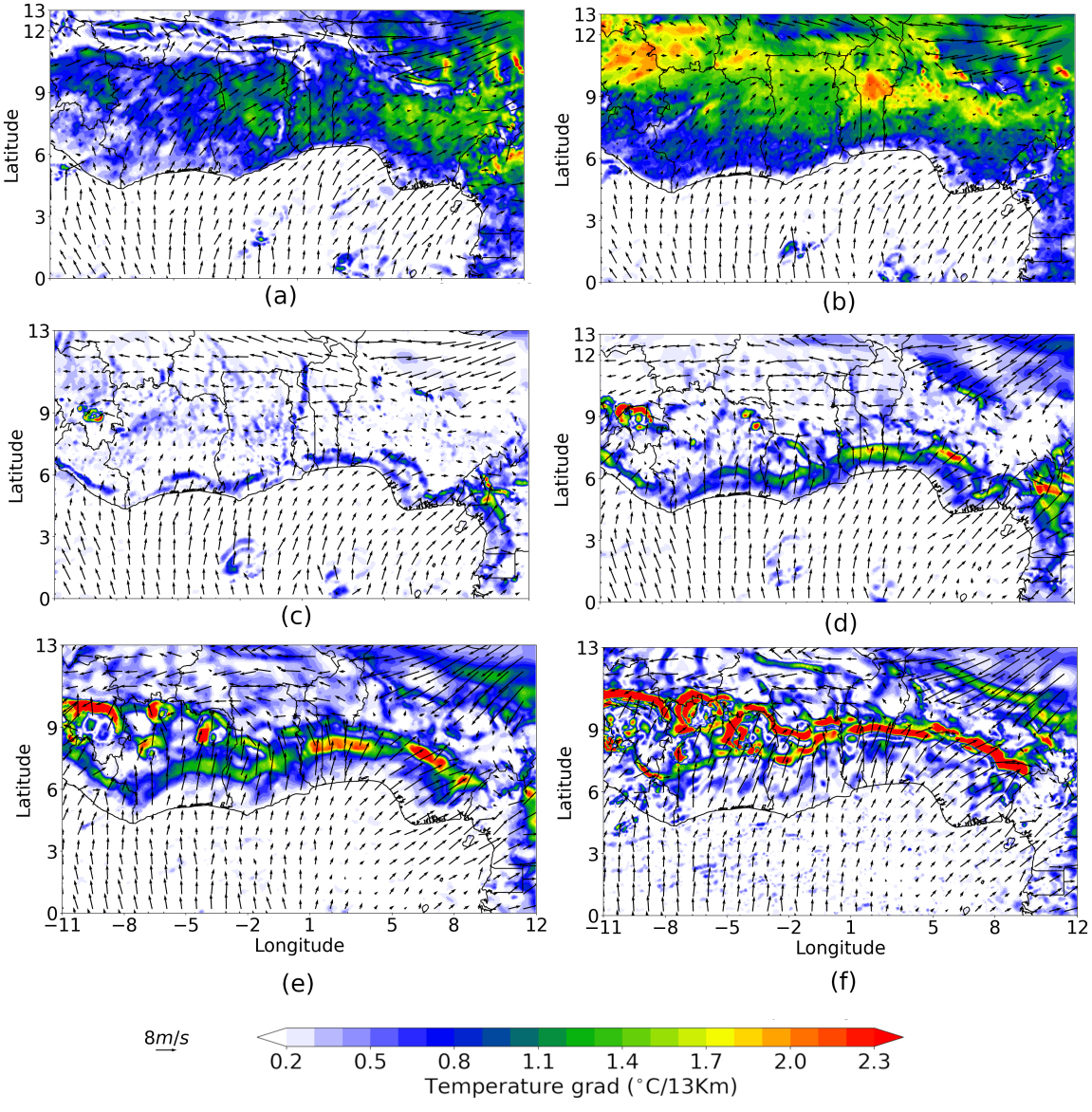

Figure 7. ICON-ART temperature gradients in the lower boundary layers (shading) and wind at 10m (arrows) at (a) 0900, (b) 1200, (c) 1500, (d) 1800, (e) 2100 and (f) 0000 UTC on 08 and 09 January 2021.

https://doi.org/10.5194/egusphere-2026-3128
Preprint. Discussion started: 23 June 2026

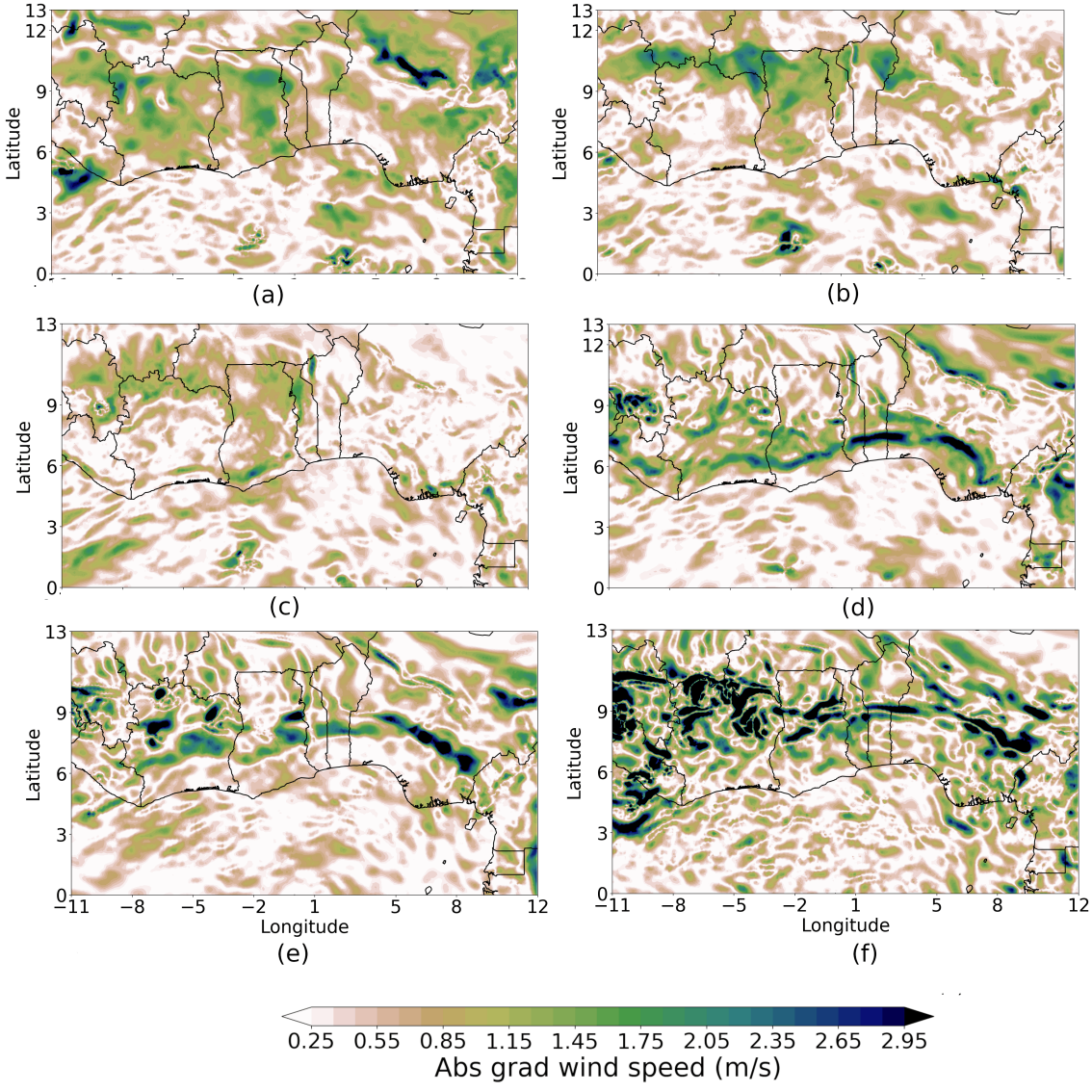

Figure 8. ICON-ART absolute value of the wind speed gradient in the lower boundary layer at (a) 0900, (b) 1200, (c) 1500, (d) 1800, (e) 2100 and (f) 0000 UTC on 08 and 09 January 2021, respectively.

https://doi.org/10.5194/egusphere-2026-3128
Preprint. Discussion started: 23 June 2026

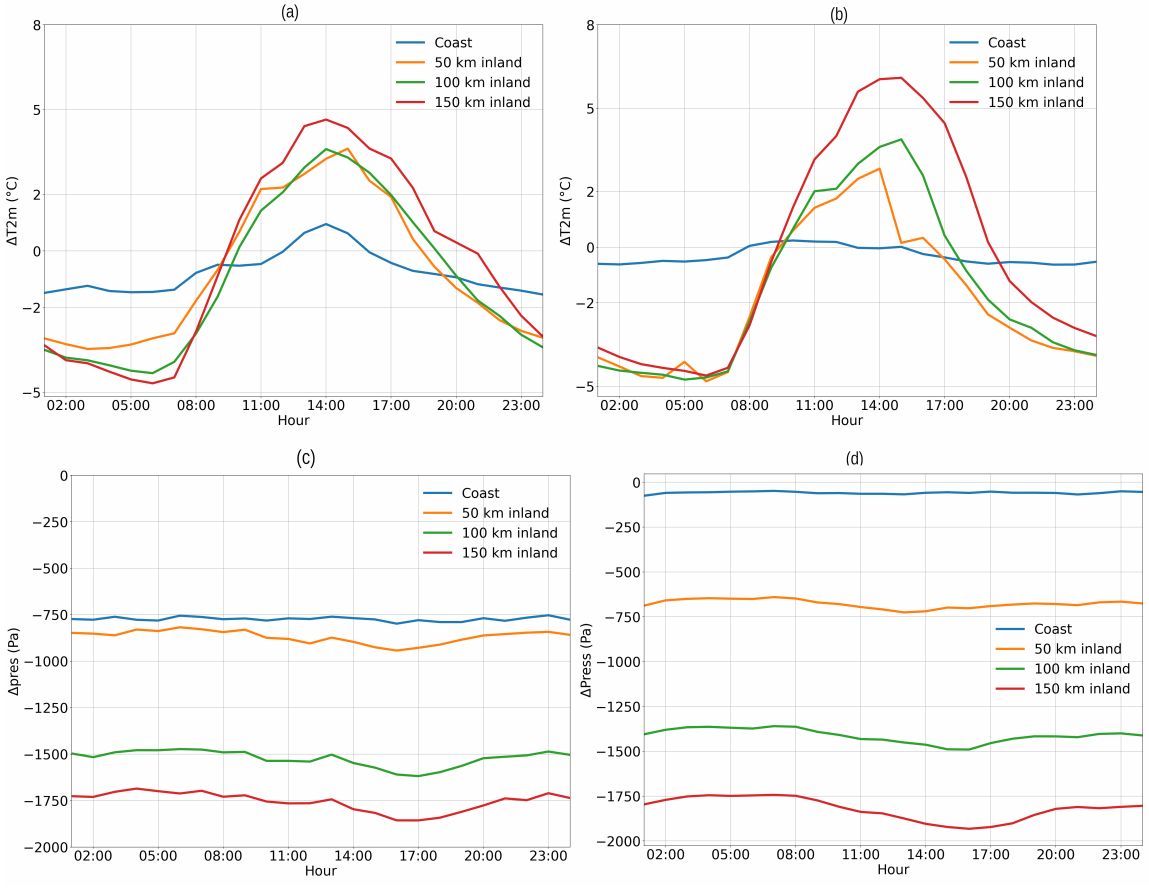

Figure 9. 2m temperature gradient (a) and (b) and pressure gradients (c) and (d) for respectively ICON and ECMWF operational analysis at a south-north of Abidjan (3.93 ° W; 5.26 ° N) perpendicular to the coast. The southernmost point is located over the Gulf of Guinea at 50 km offshore and inland points at distance of 50 km, 100 km, and 150 km

https://doi.org/10.5194/egusphere-2026-3128
Preprint. Discussion started: 23 June 2026

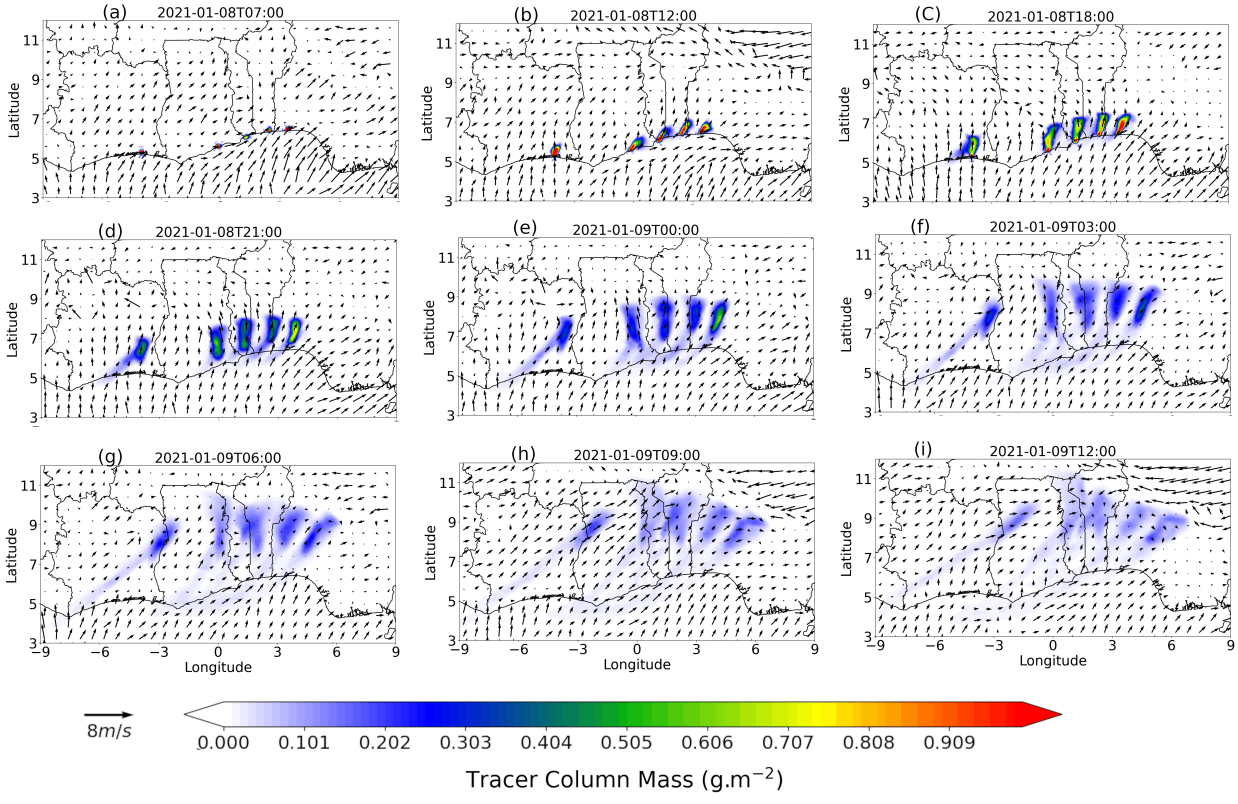

Figure 10. Total pollutant column mass and 10m wind arrows at (a) 0700, (b) 1200, (c) 1800, (d) 2100, (e) 0000, (f) 0300, (g) 0600, (h) 0900 and (i) 1200 UTC on 08 and 09 January 2021, respectively. Pollutants are emitted from point sources in the main coastal cities (Abidjan, Accra, Lomé, Cotonou and Lagos) from 0600 UTC to 1800 UTC on 08 January 2021.

https://doi.org/10.5194/egusphere-2026-3128
Preprint. Discussion started: 23 June 2026

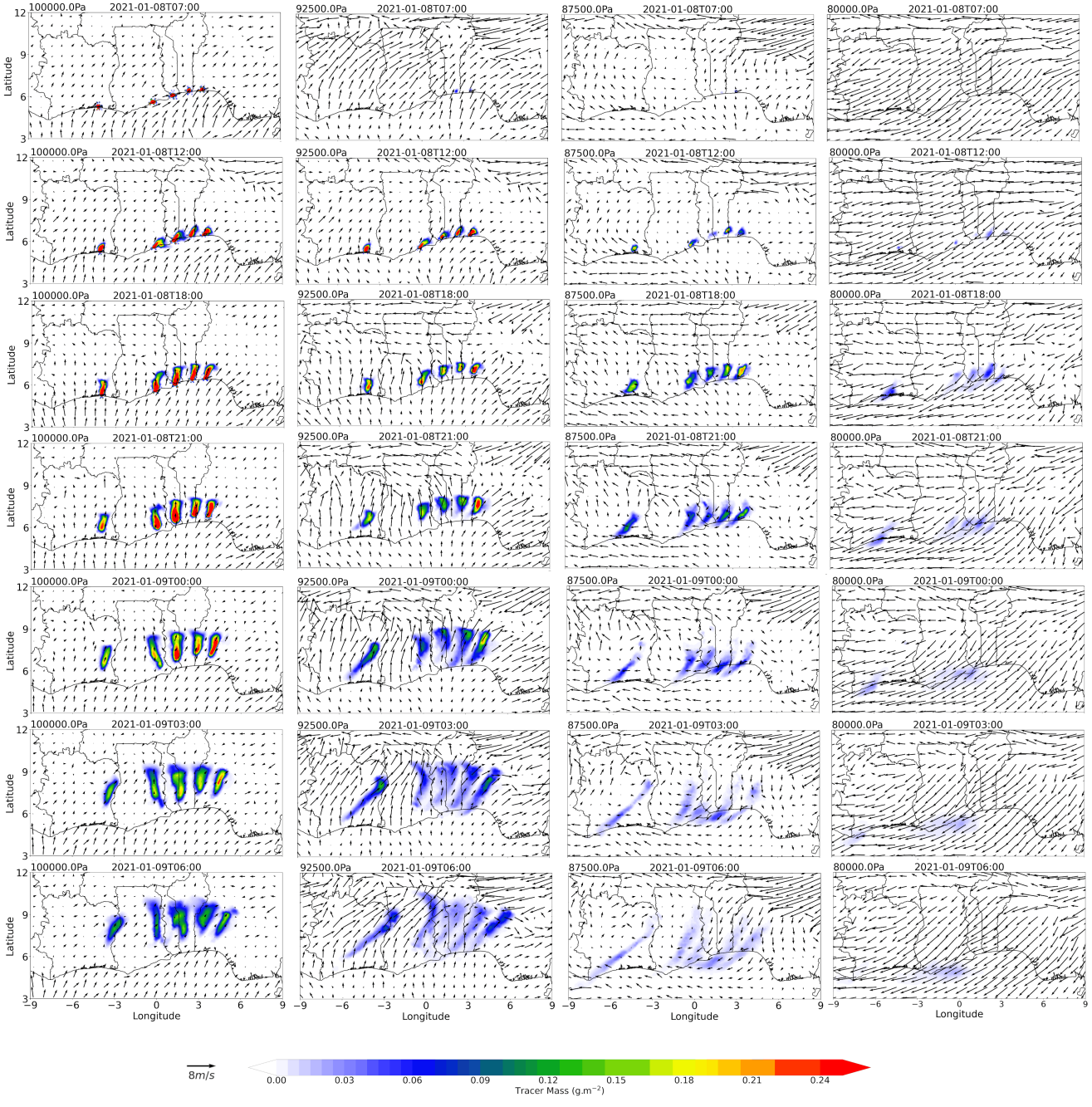

Figure 11. Evolution of pollutant plume transport within the LSB layer and wind (arrow) within each of the layers considered at various hours (from top to down) 0700 (first raw), 1200 (second raw), 1800 (third raw), 2100 (fourth raw), 0000 (fifth raw), 0300 (sixth raw), and 0600 (seventh raw) within various atmospheric layers (from left to right) at 1000 hPa, (first column) 925 hPa (second column), 875 hPa, and (third column) 800 hPa (fourth column).

https://doi.org/10.5194/egusphere-2026-3128
Preprint. Discussion started: 23 June 2026

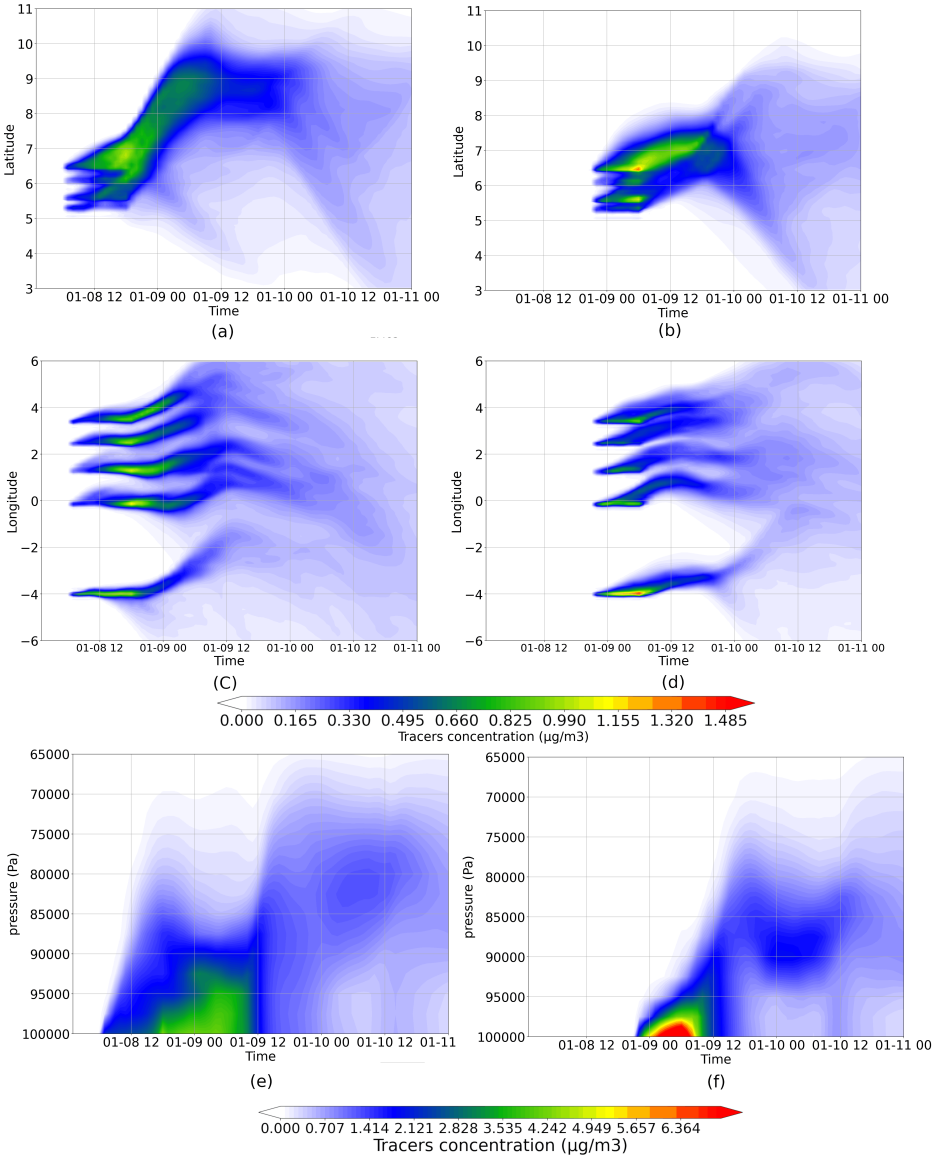

Figure 12. Time evolution of pollutant plume during 08–10 January 2021 (horizontal axis). Latitudinal evolution of column mass (mean between 6°W and 6°E) for (a) daytime and (b) nighttime emissions. Zonal evolution of column mass (mean between 3°N and 11°N) for (c) daytime emissions and (d) nighttime emissions. Vertical evolution (mean 6° W and 6°E - 3°N - 11°N) for (e) daytime emissions and (f) nighttime emissions. Pollutants are emitted from point sources in the main coastal cities (Abidjan, Accra, Lomé, Cotonou and Lagos) from 0600 UTC to 1800 UTC on 08 January 2021 for daytime emissions and from 2100 UTC to 0600 UTC on 08 January 2021 for the nighttime emissions.

https://doi.org/10.5194/egusphere-2026-3128
Preprint. Discussion started: 23 June 2026

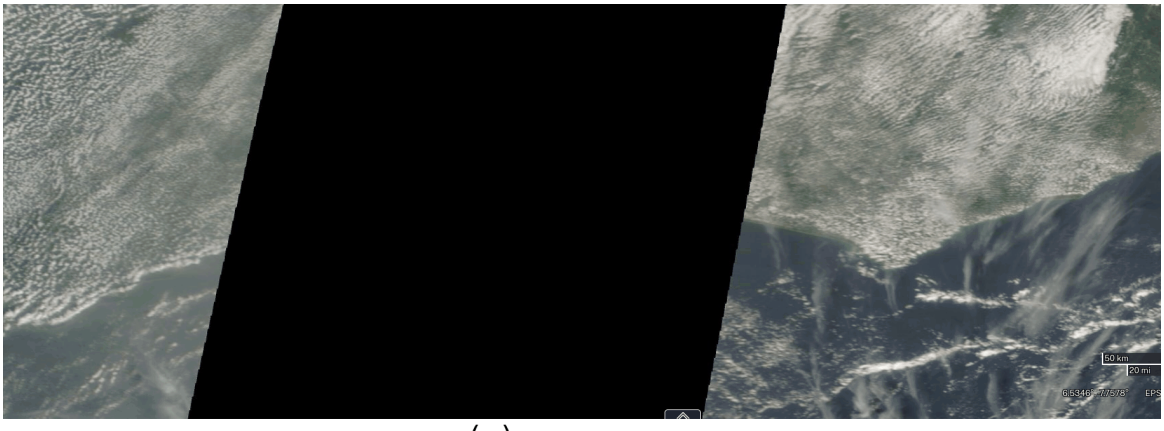

(a)

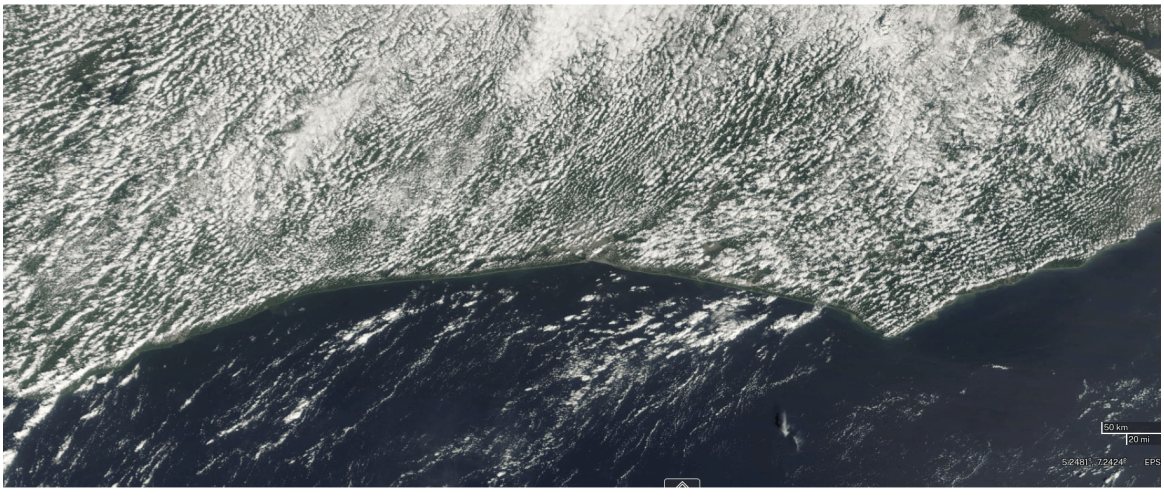

(b)

https://doi.org/10.5194/egusphere-2026-3128
Preprint. Discussion started: 23 June 2026

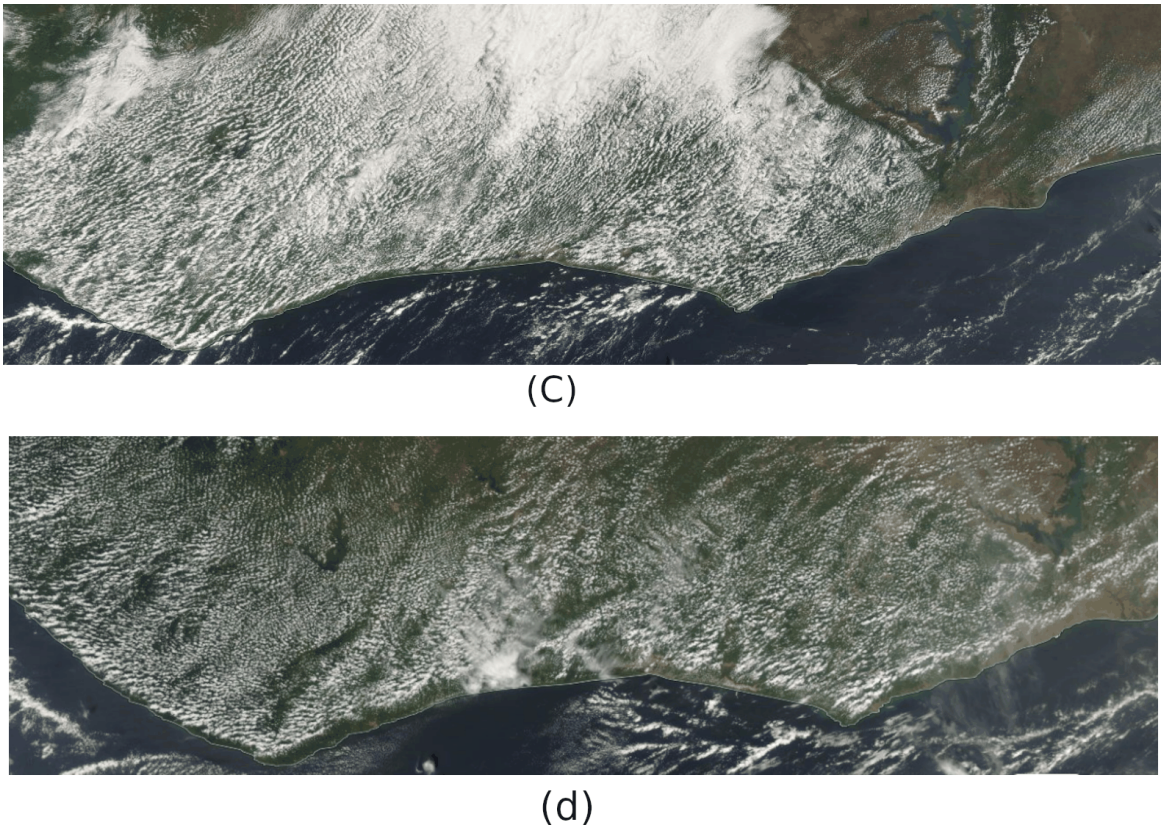

Figure A1. Observational evidence of the LSB occurrence from MODIS cloud cover (a, c) AQUA and (b, d) TERRA for the case study on 09 and 10 January 2021.

https://doi.org/10.5194/egusphere-2026-3128
Preprint. Discussion started: 23 June 2026

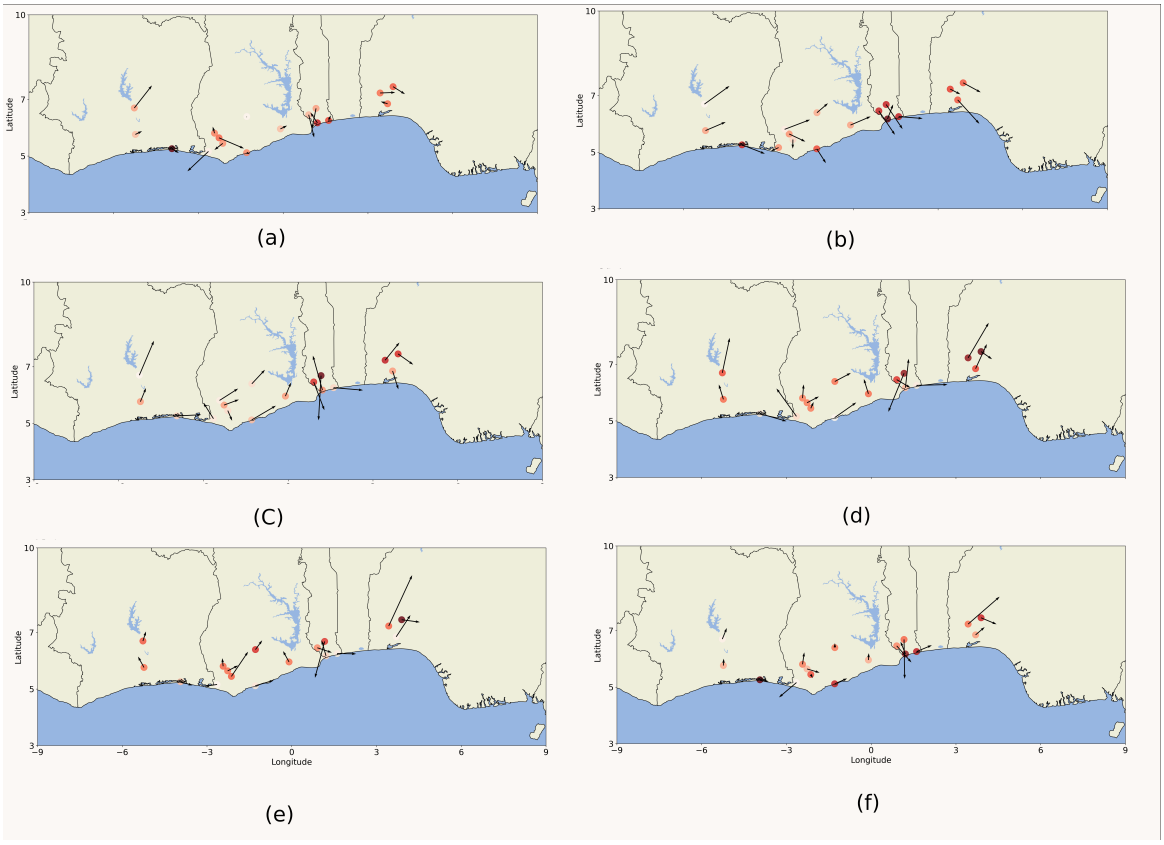

https://doi.org/10.5194/egusphere-2026-3128
Preprint. Discussion started: 23 June 2026

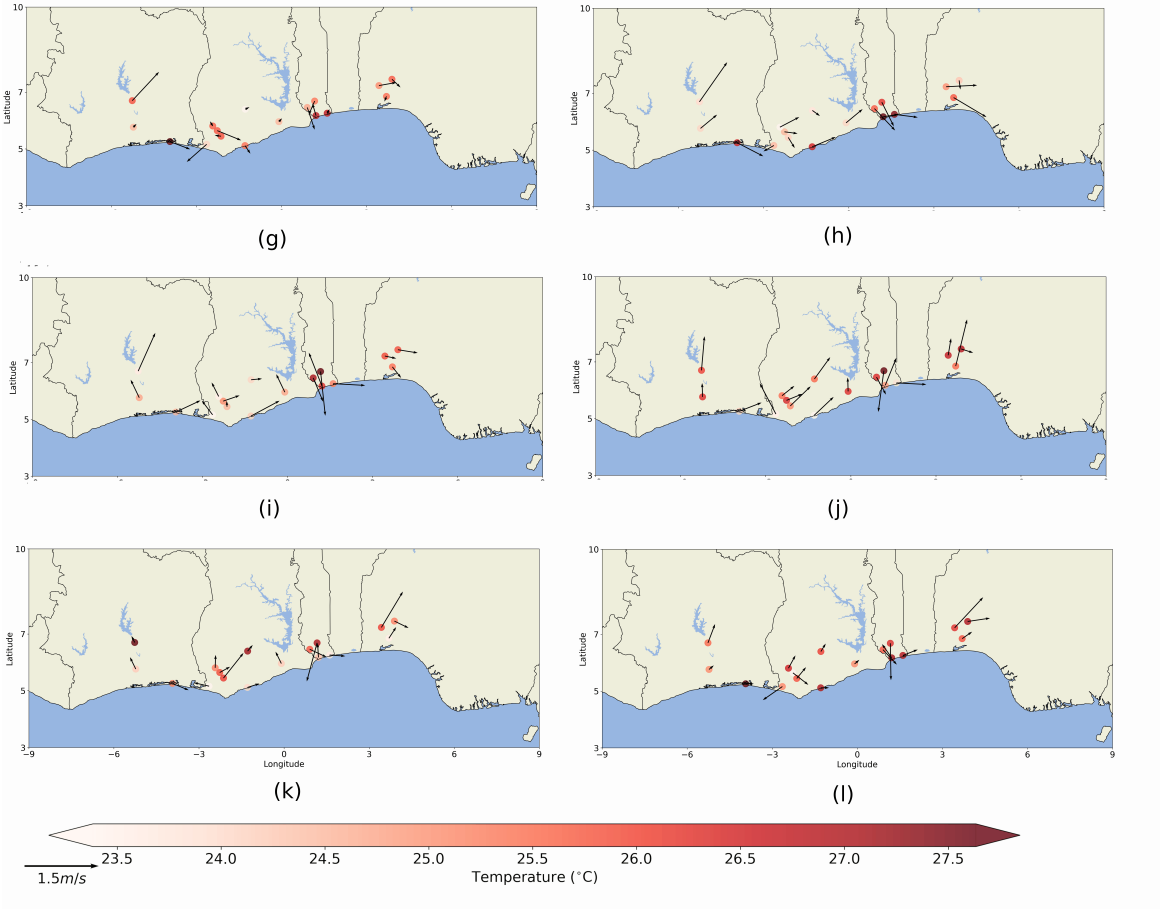

Figure A2. 17 TAHMO stations showing hourly wind arrows and shaded temperature at (a, g) 0600, (b, h) 0900, (c, i) 1200, (d and j) 1500, (e, k) 1800 and (f, l) 2100 LT on 08 and 09 January 2021 respectively.

https://doi.org/10.5194/egusphere-2026-3128
Preprint. Discussion started: 23 June 2026

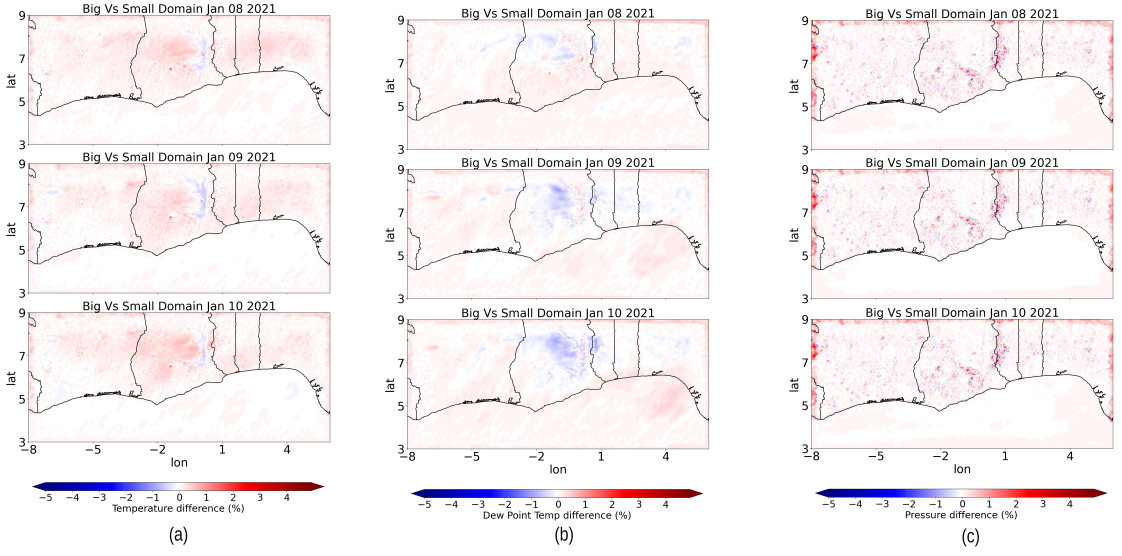

Figure A3. Daily mean difference in percentage between the main domain and the nested domain for (a) 2m temperature, (b) dew point temperature, and (c) mean sea-level pressure during 08, 09 and 10 January 2021.

https://doi.org/10.5194/egusphere-2026-3128
Preprint. Discussion started: 23 June 2026

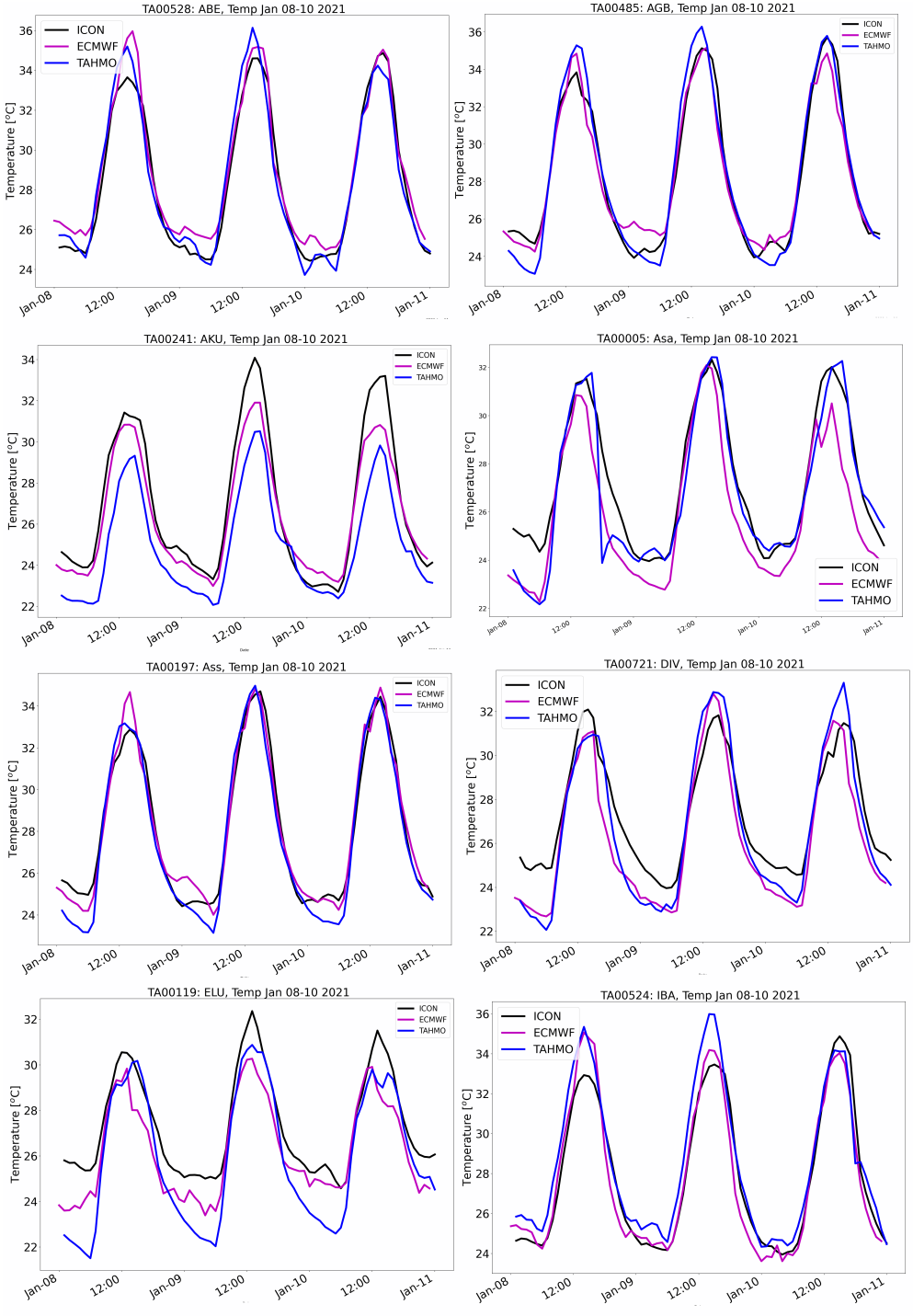

https://doi.org/10.5194/egusphere-2026-3128
Preprint. Discussion started: 23 June 2026

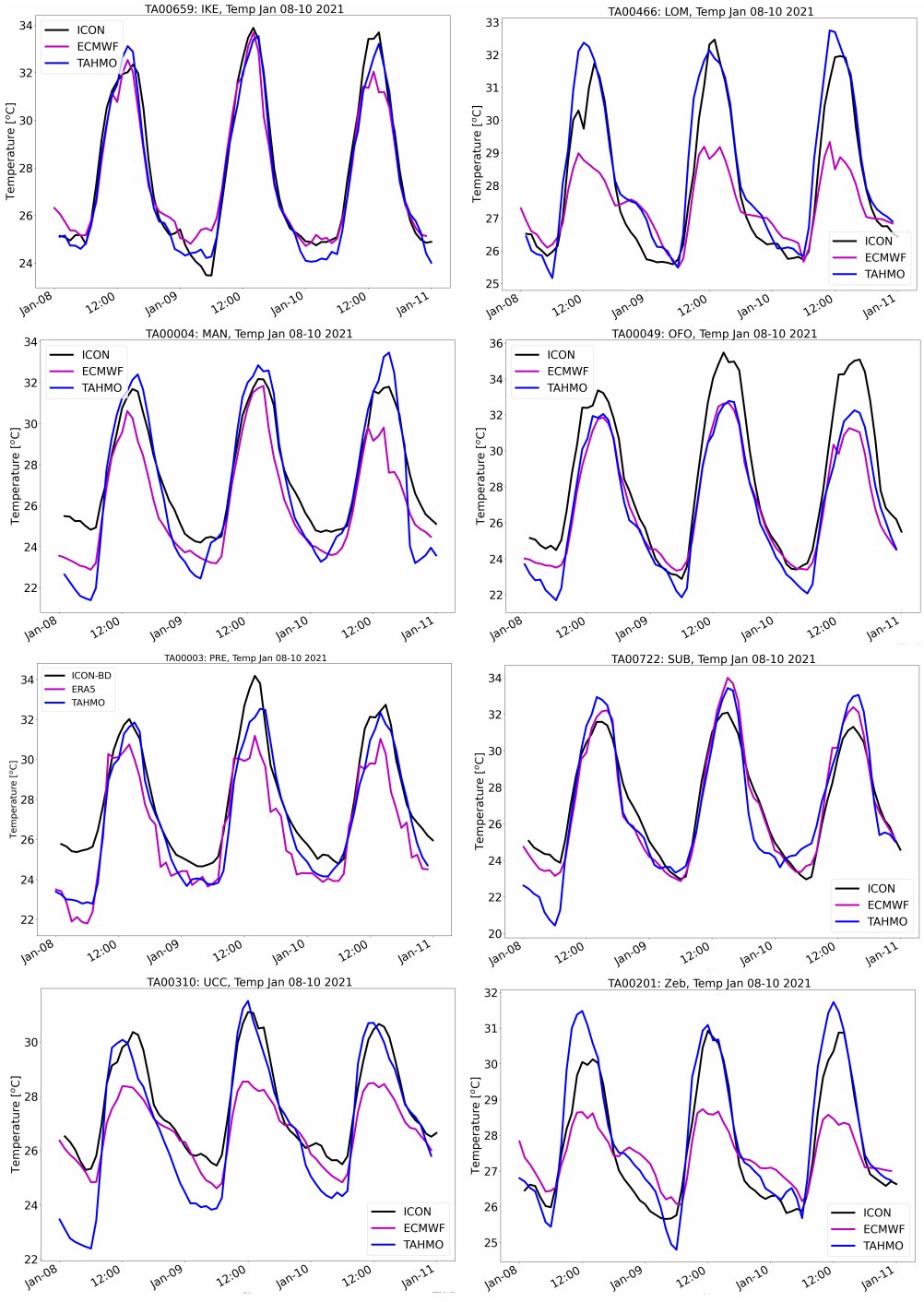

https://doi.org/10.5194/egusphere-2026-3128
Preprint. Discussion started: 23 June 2026

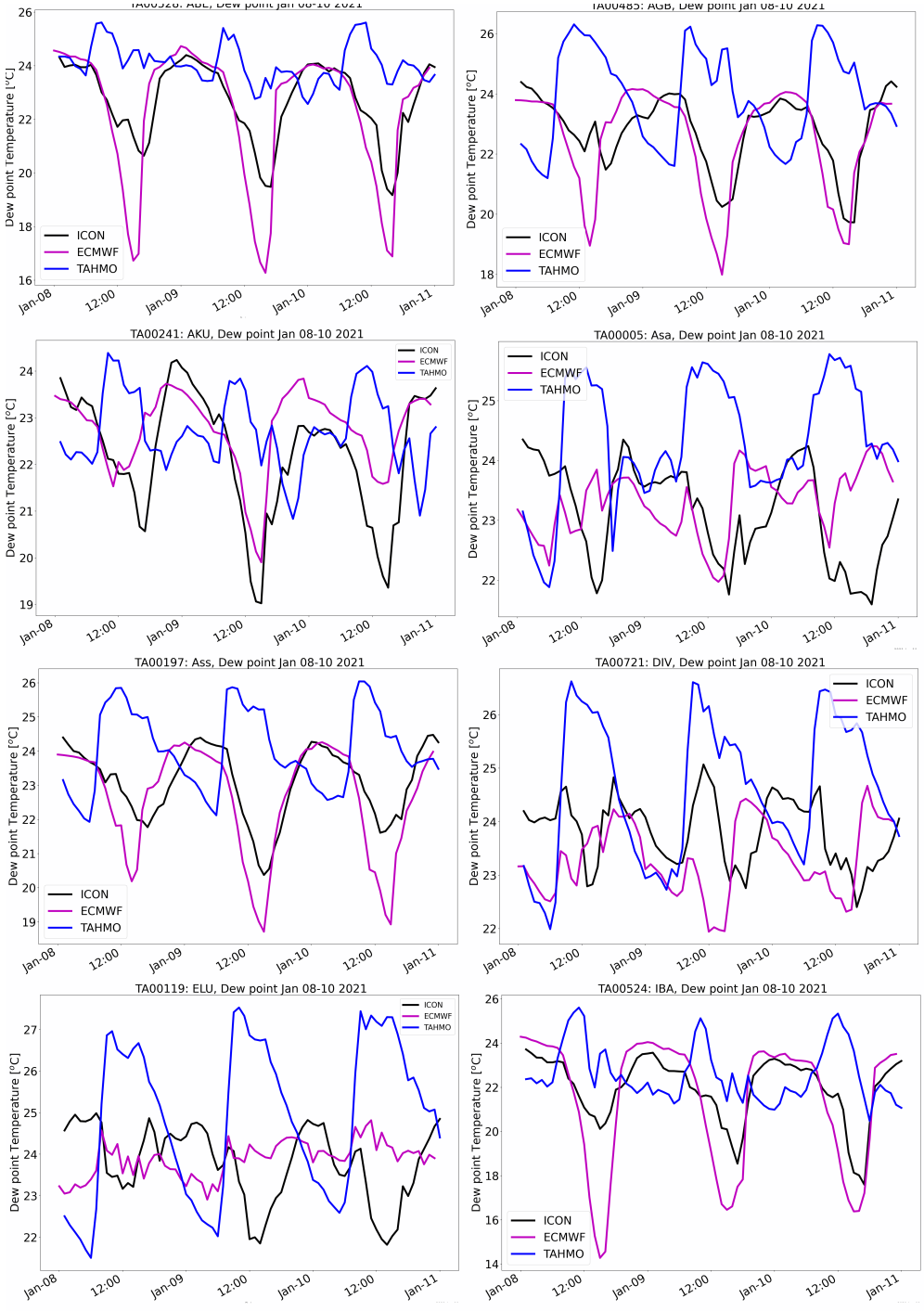

https://doi.org/10.5194/egusphere-2026-3128
Preprint. Discussion started: 23 June 2026

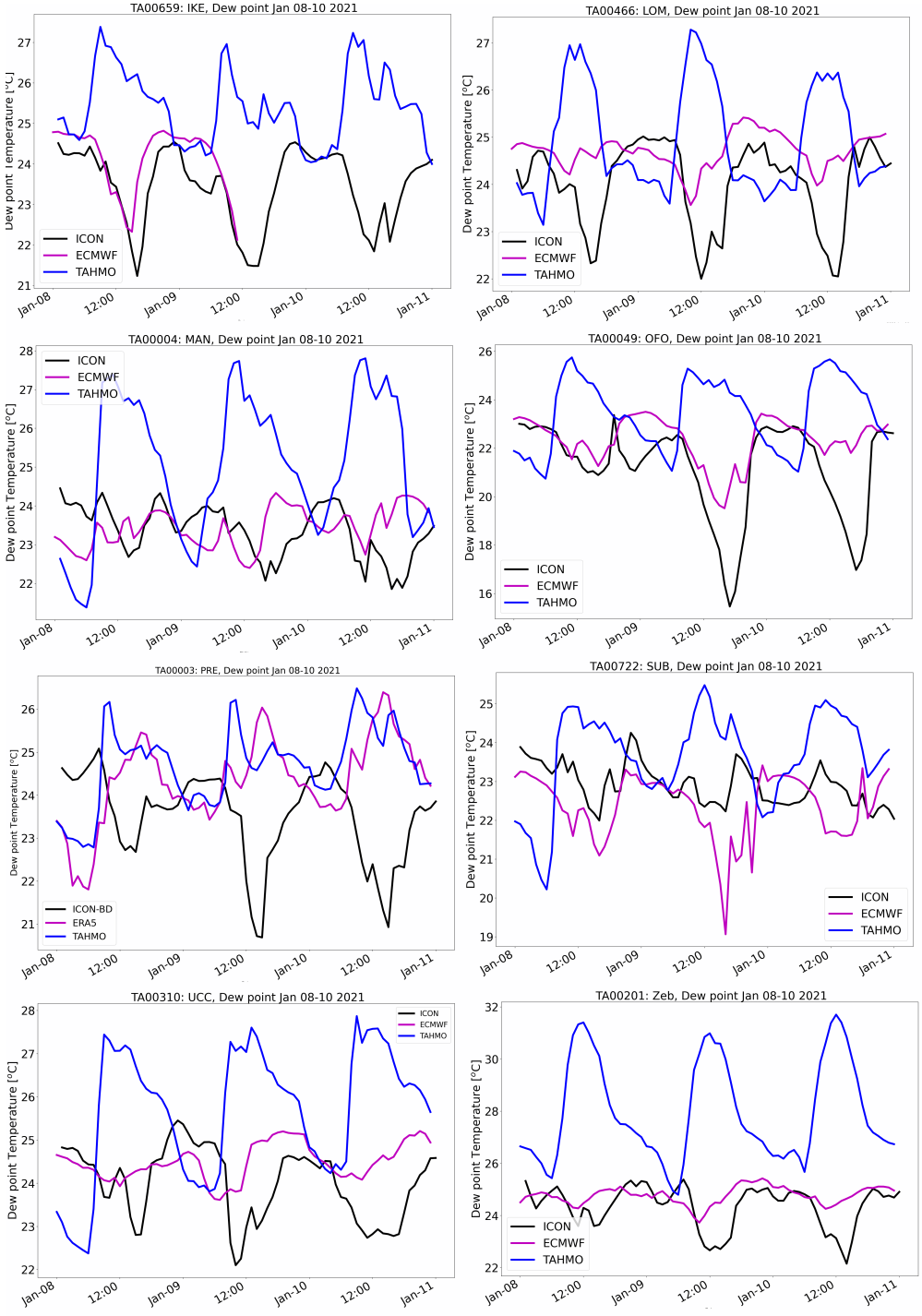

https://doi.org/10.5194/egusphere-2026-3128
Preprint. Discussion started: 23 June 2026

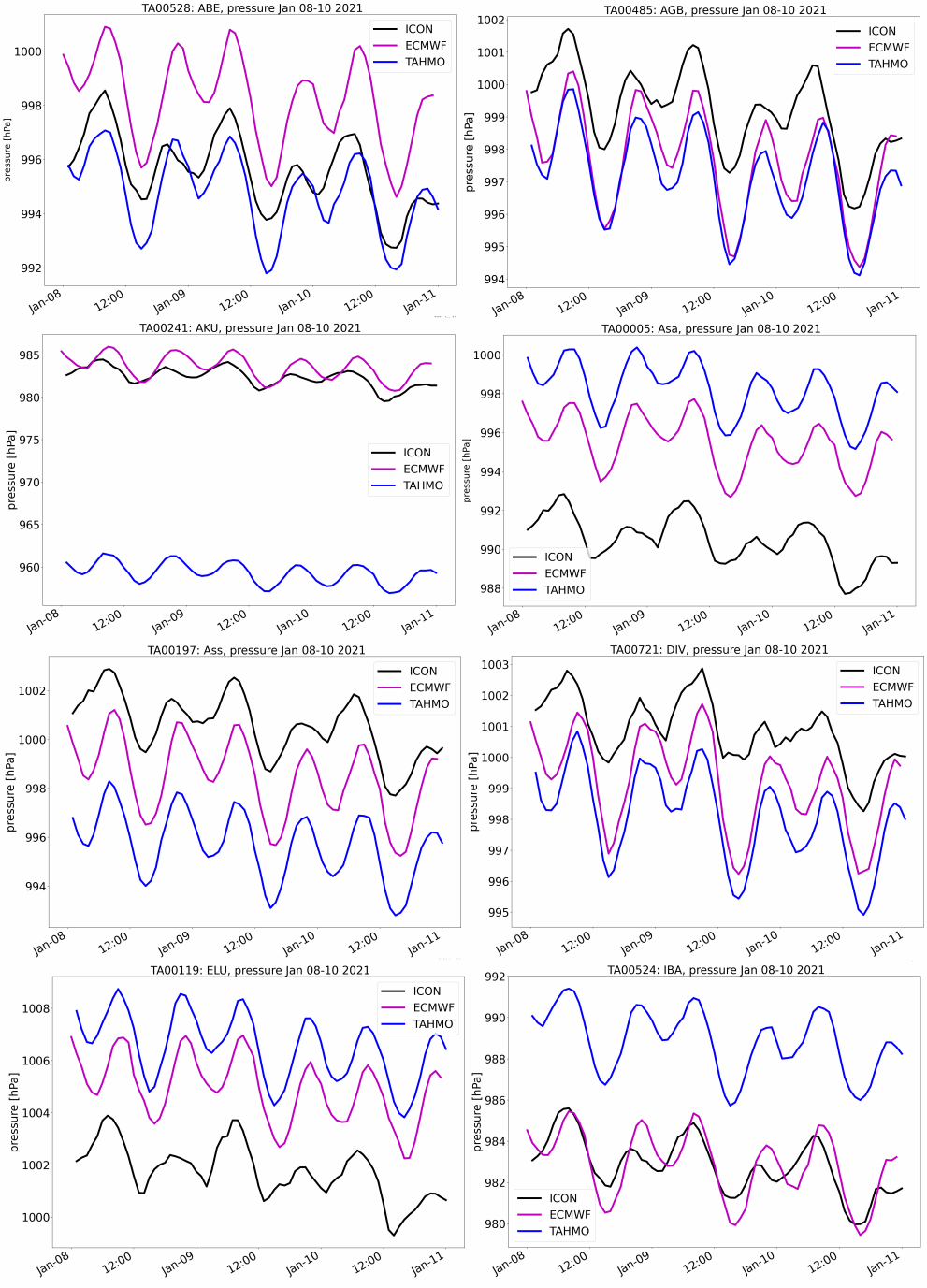

https://doi.org/10.5194/egusphere-2026-3128
Preprint. Discussion started: 23 June 2026

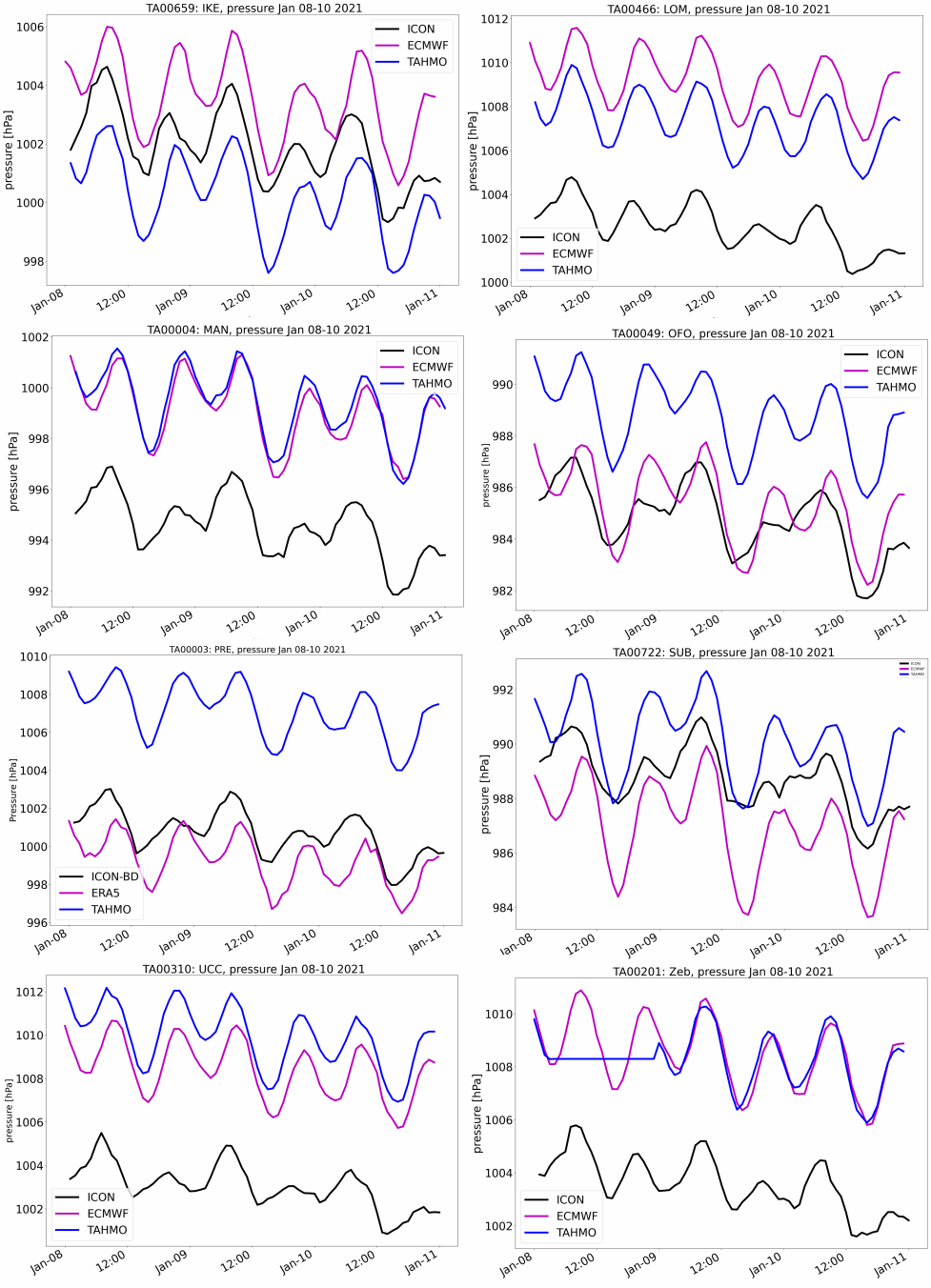

https://doi.org/10.5194/egusphere-2026-3128
Preprint. Discussion started: 23 June 2026

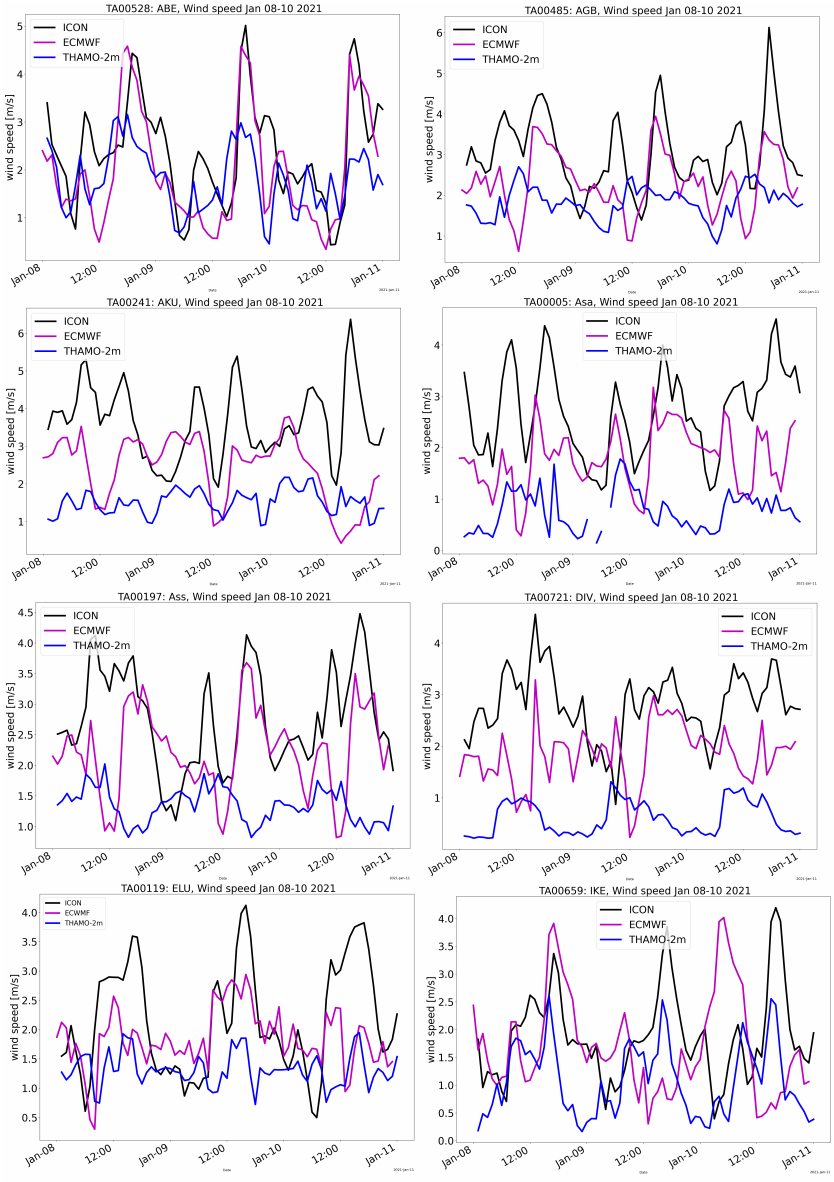

https://doi.org/10.5194/egusphere-2026-3128
Preprint. Discussion started: 23 June 2026

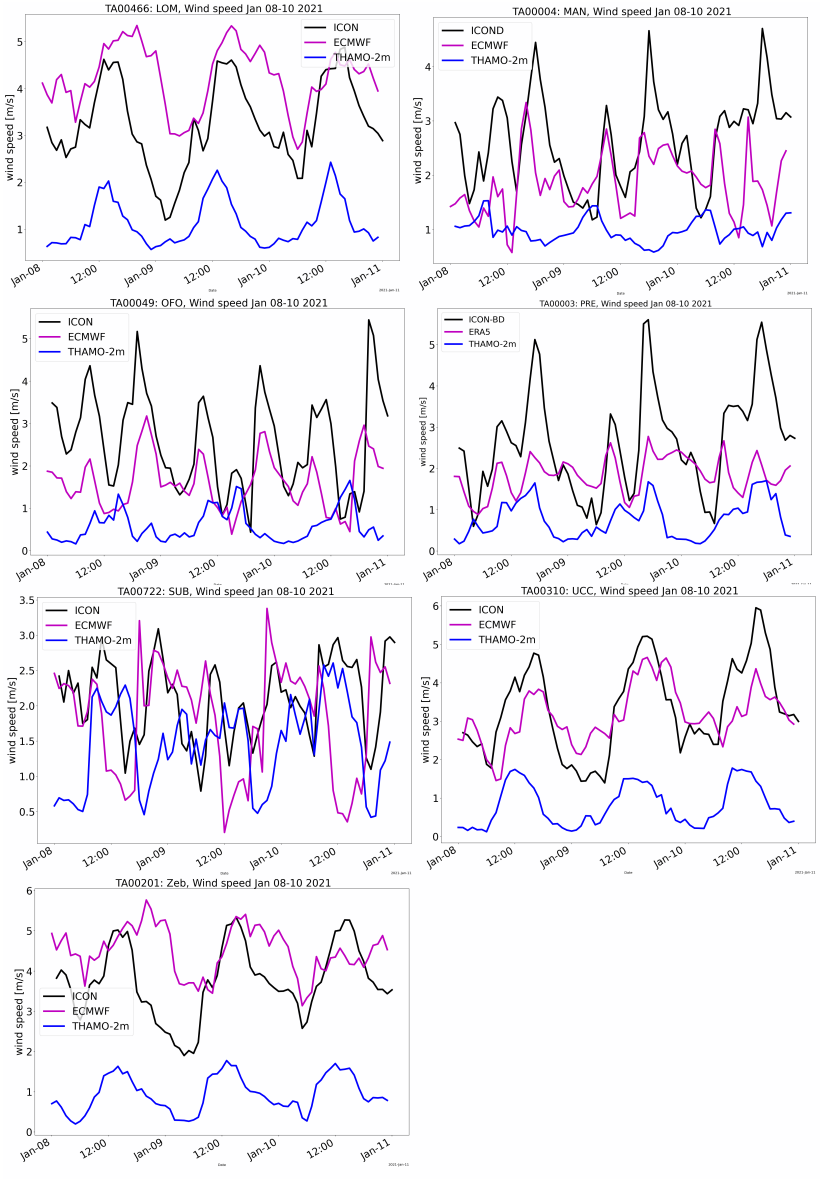

Figure A4. Comparison of hourly time series of variables of T2m, dew point temperature, surface pressure and wind speed at 16 TAHMO stations during 08 to 10 January 2021.

https://doi.org/10.5194/egusphere-2026-3128
Preprint. Discussion started: 23 June 2026

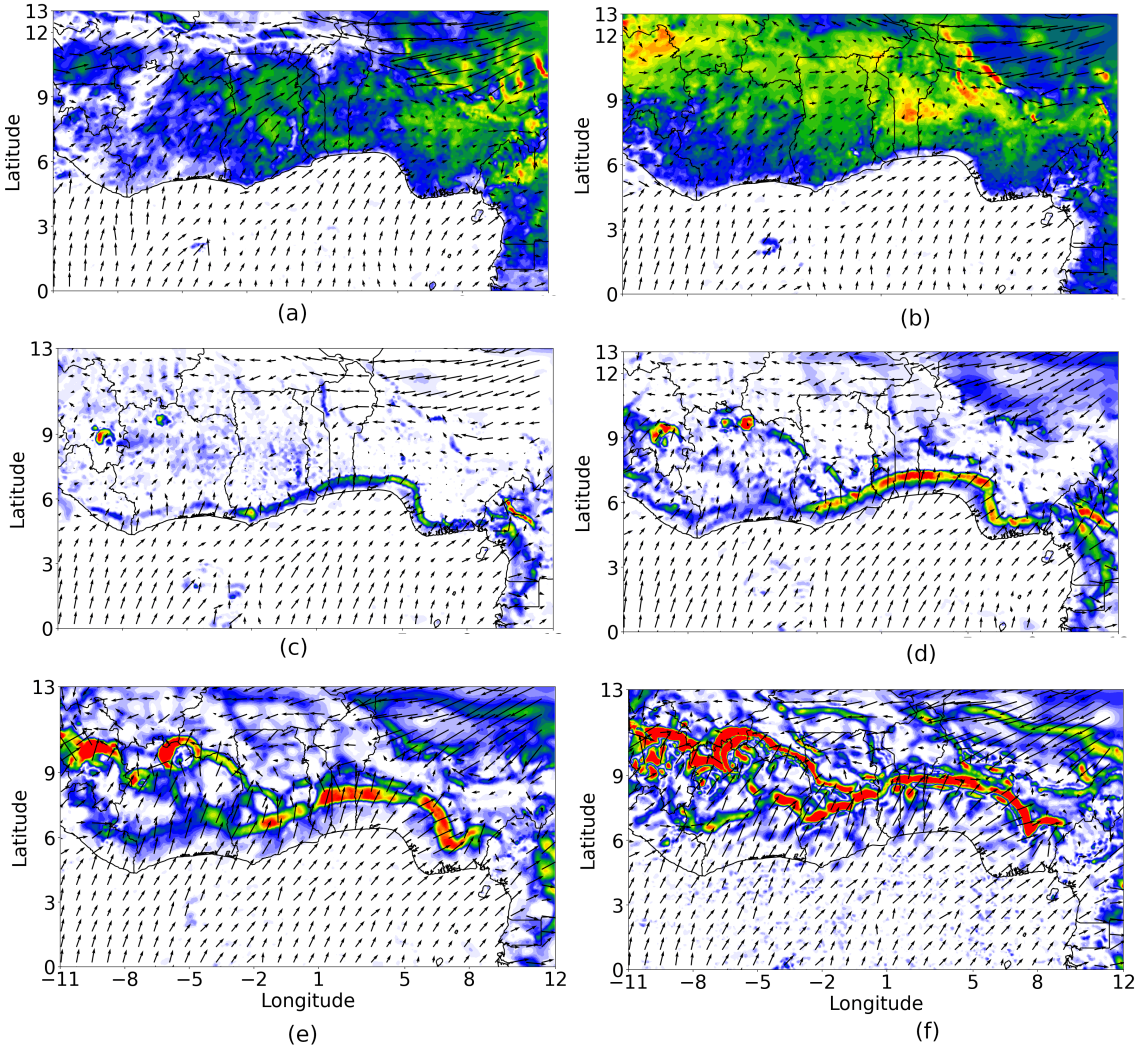

https://doi.org/10.5194/egusphere-2026-3128
Preprint. Discussion started: 23 June 2026

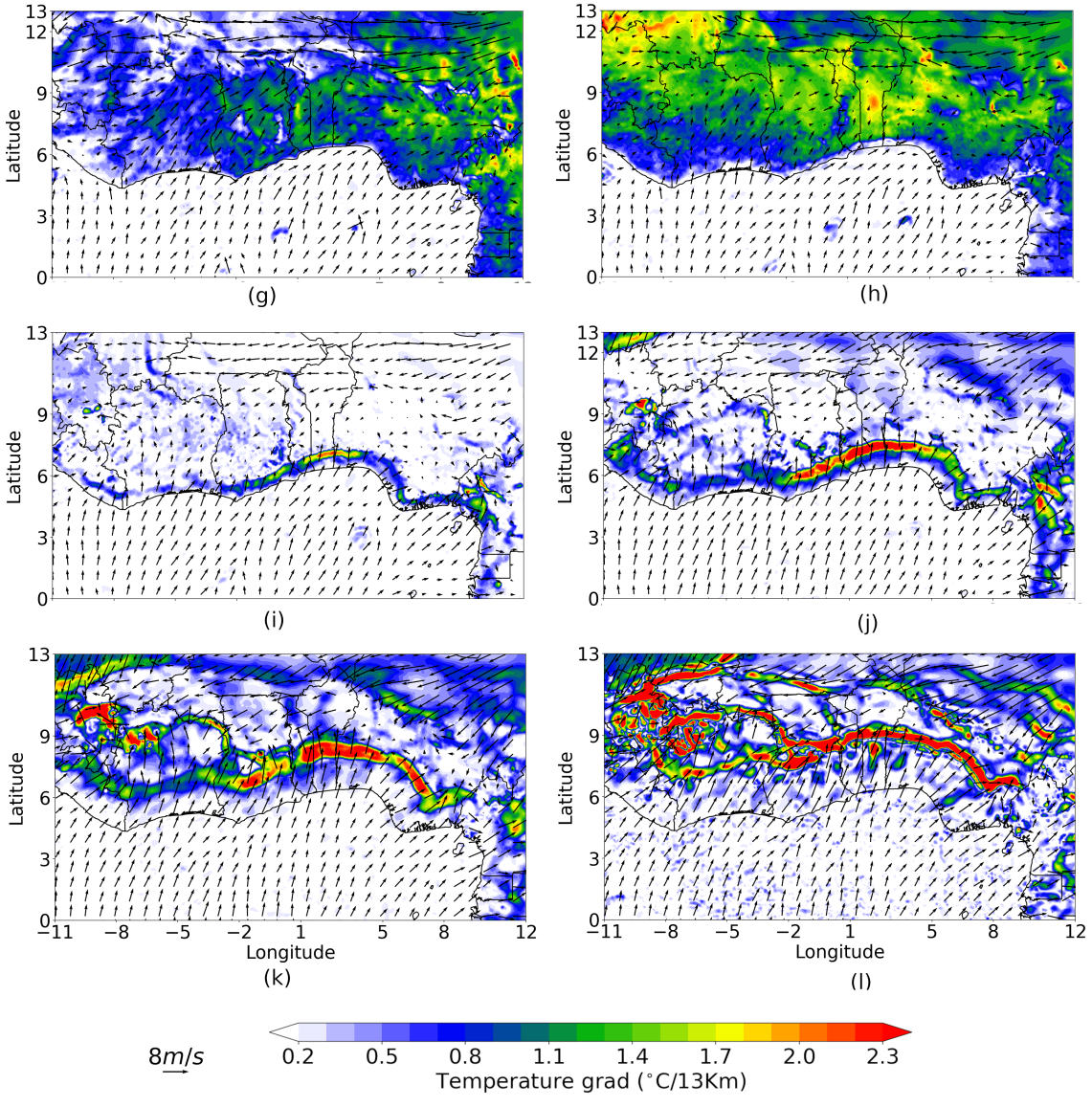

Figure A5. Temperature gradients and wind arrows at (a, g) 0900, (b, h) 1200, (c, i) 1500, (d, j) 1800, (e, k) 2100 and (f, l) 0000 UTC in the lower boundary layer associated with LSB occurrence on 09 and 10 January 2021.

https://doi.org/10.5194/egusphere-2026-3128
Preprint. Discussion started: 23 June 2026

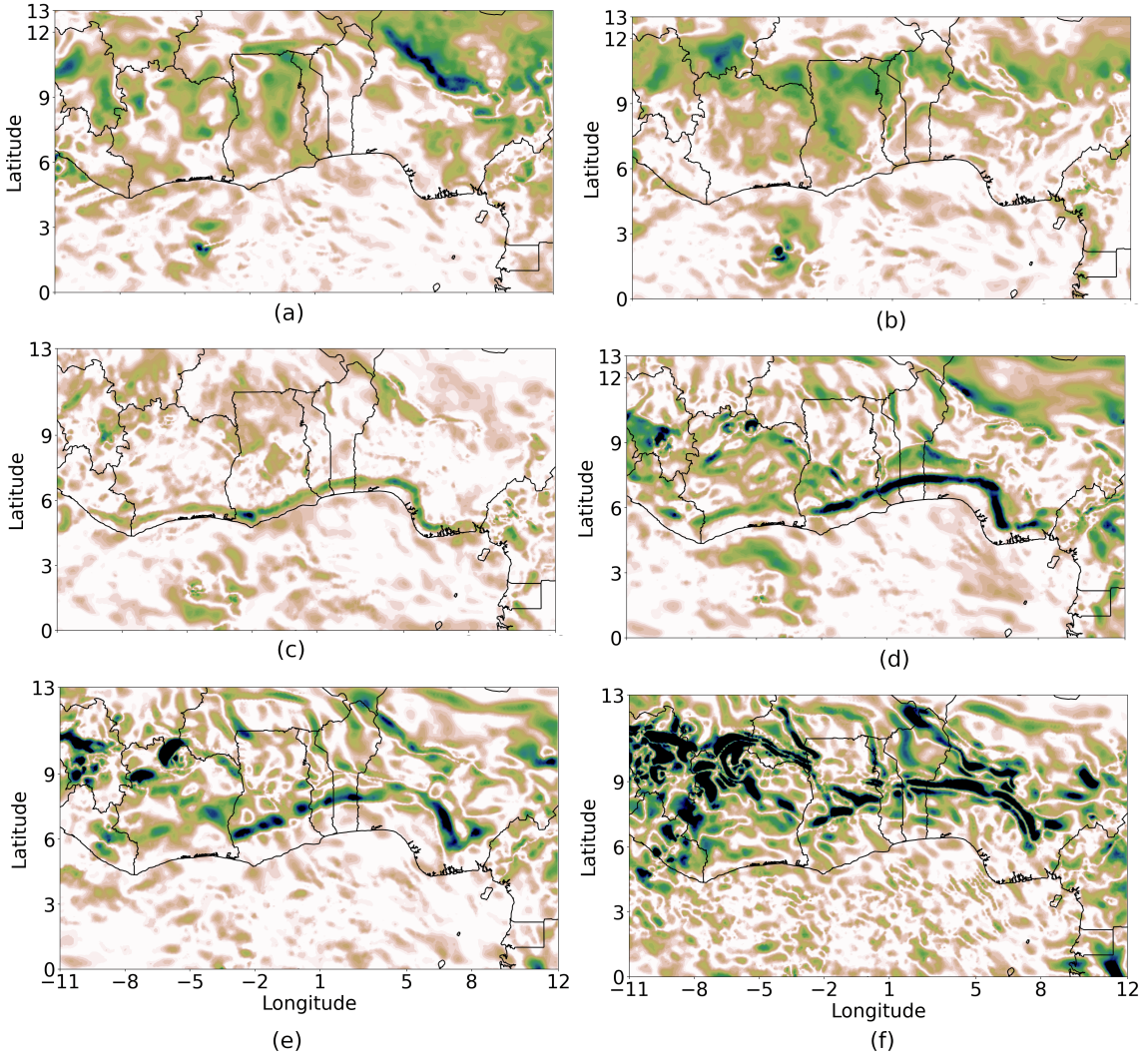

https://doi.org/10.5194/egusphere-2026-3128
Preprint. Discussion started: 23 June 2026

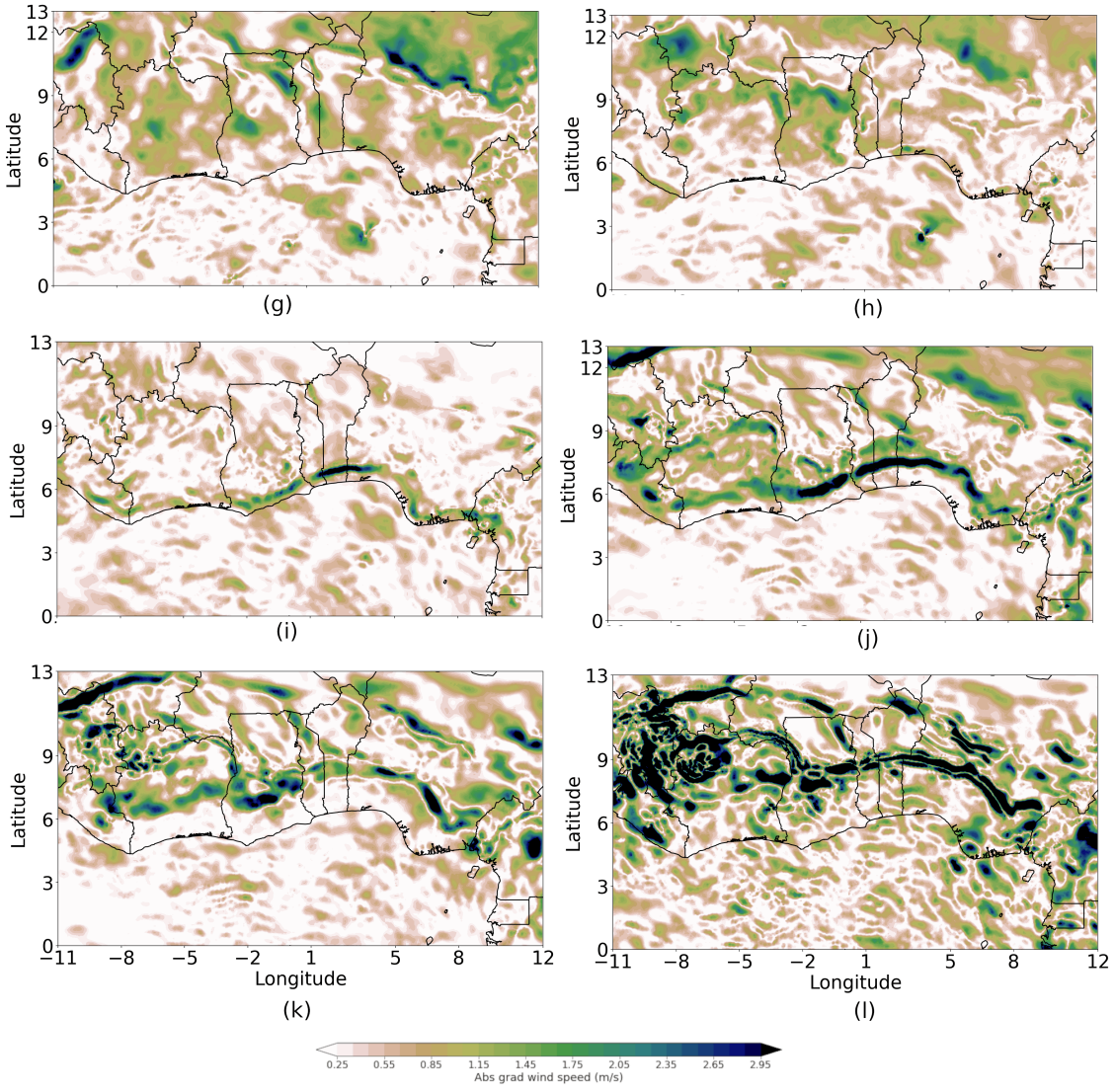

Figure A6. Wind speed gradient (a, g) 0900, (b, h) 1200, (c, i) 1500, (d, j) 1800, (e, k) 2100 and (f, l) 0000 UTC in the lower boundary layer associated with LSB occurrence on 09 and 10 January 2021.

https://doi.org/10.5194/egusphere-2026-3128
Preprint. Discussion started: 23 June 2026

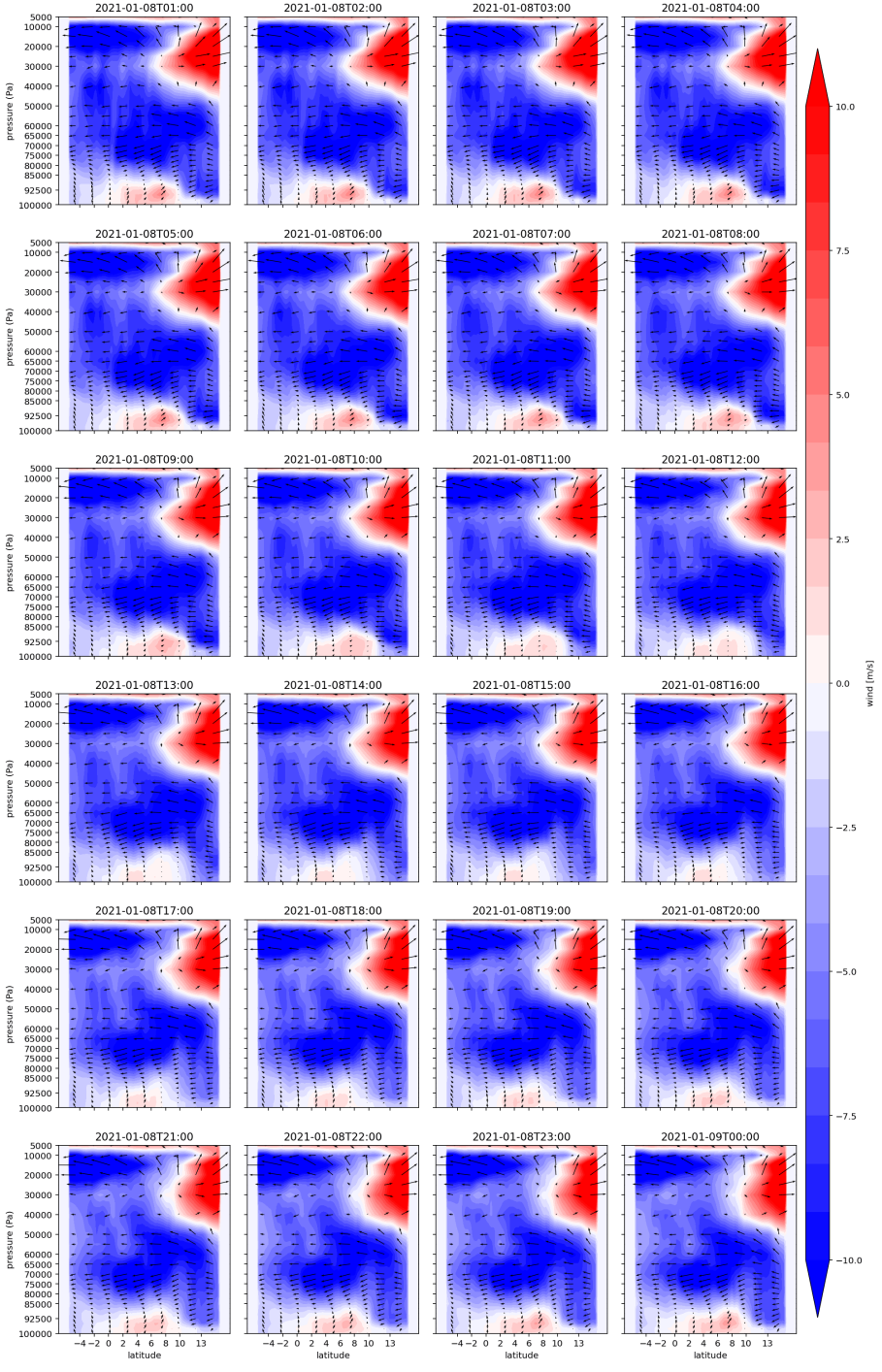

Figure A7. Hourly wind speed vertical distribution during 8 January 2021 average between 12° W -12° E.

https://doi.org/10.5194/egusphere-2026-3128
Preprint. Discussion started: 23 June 2026

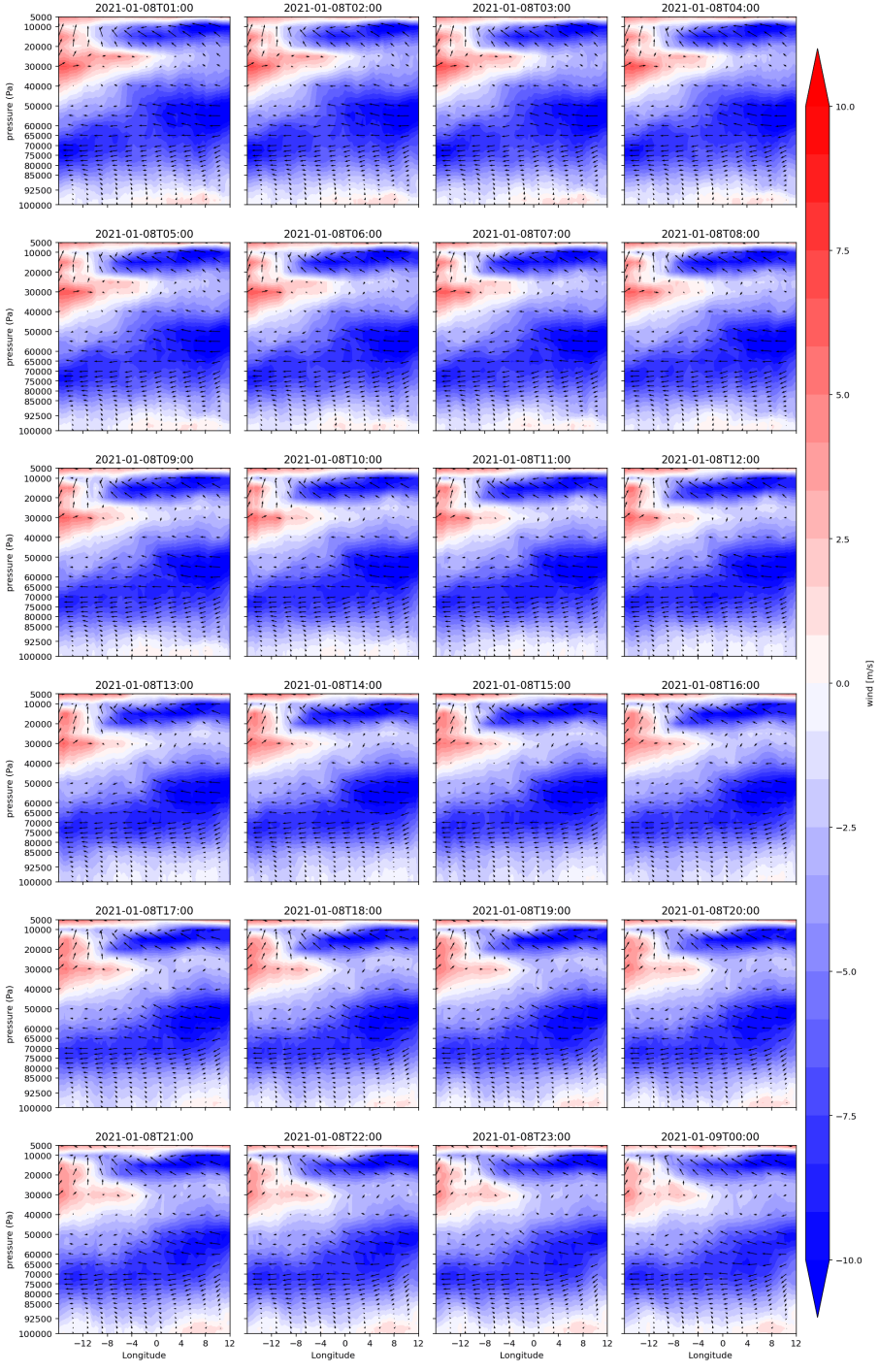

Figure A8. Hourly wind speed vertical distribution during 8 January 2021 average between 4°S and 13° N.

https://doi.org/10.5194/egusphere-2026-3128
Preprint. Discussion started: 23 June 2026

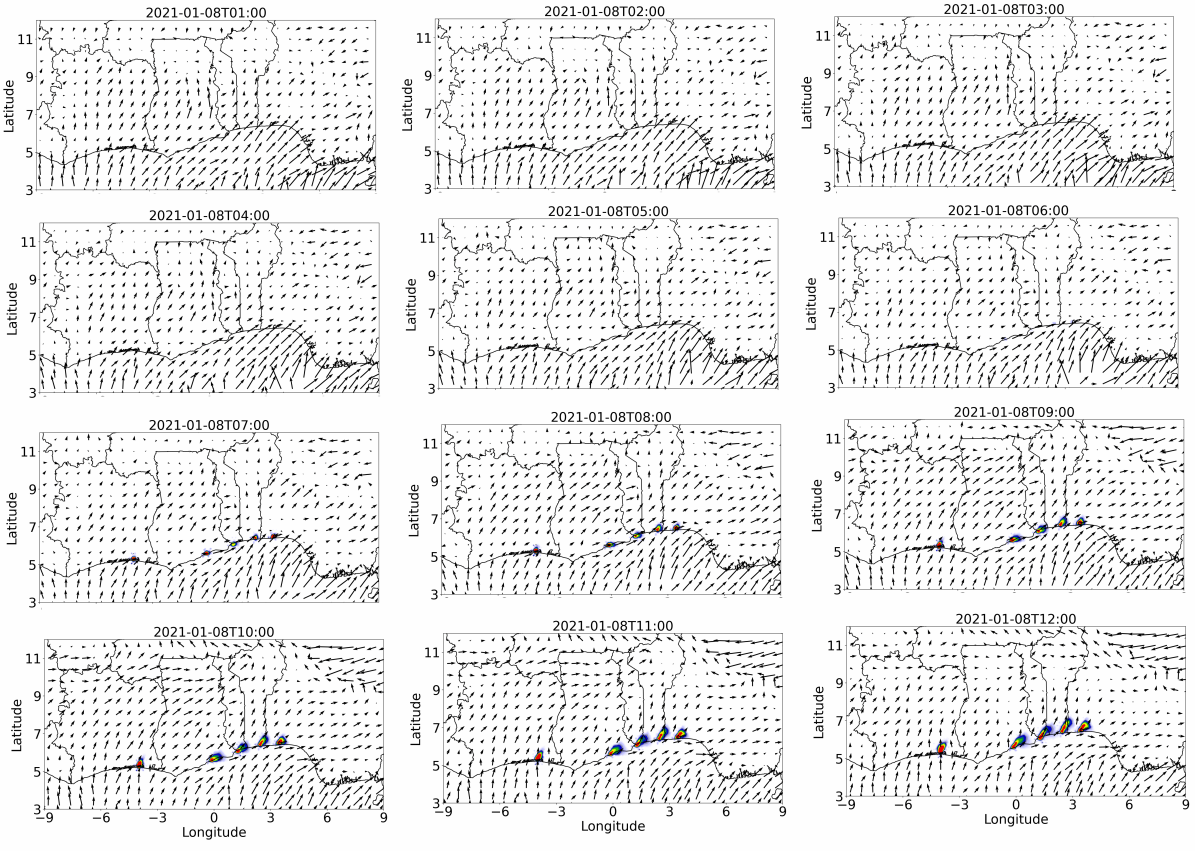

https://doi.org/10.5194/egusphere-2026-3128
Preprint. Discussion started: 23 June 2026

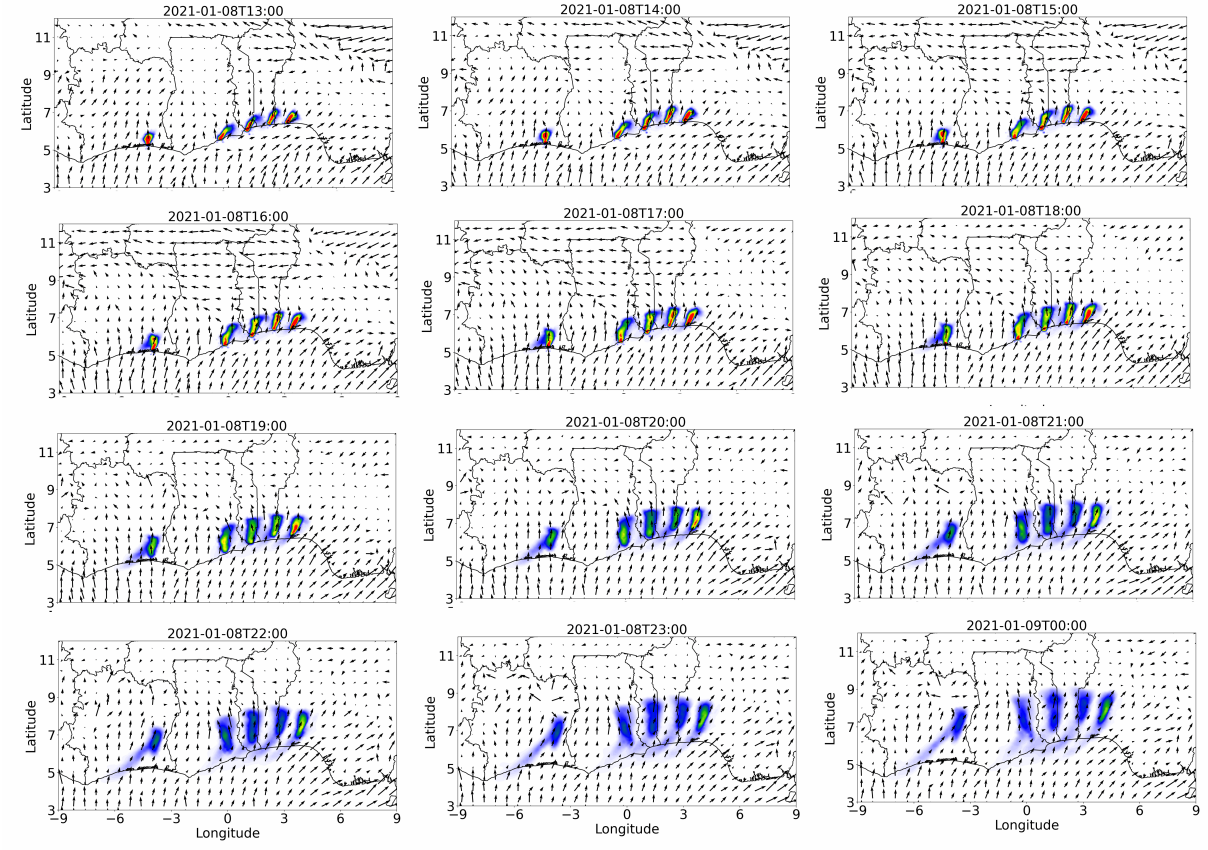

https://doi.org/10.5194/egusphere-2026-3128
Preprint. Discussion started: 23 June 2026

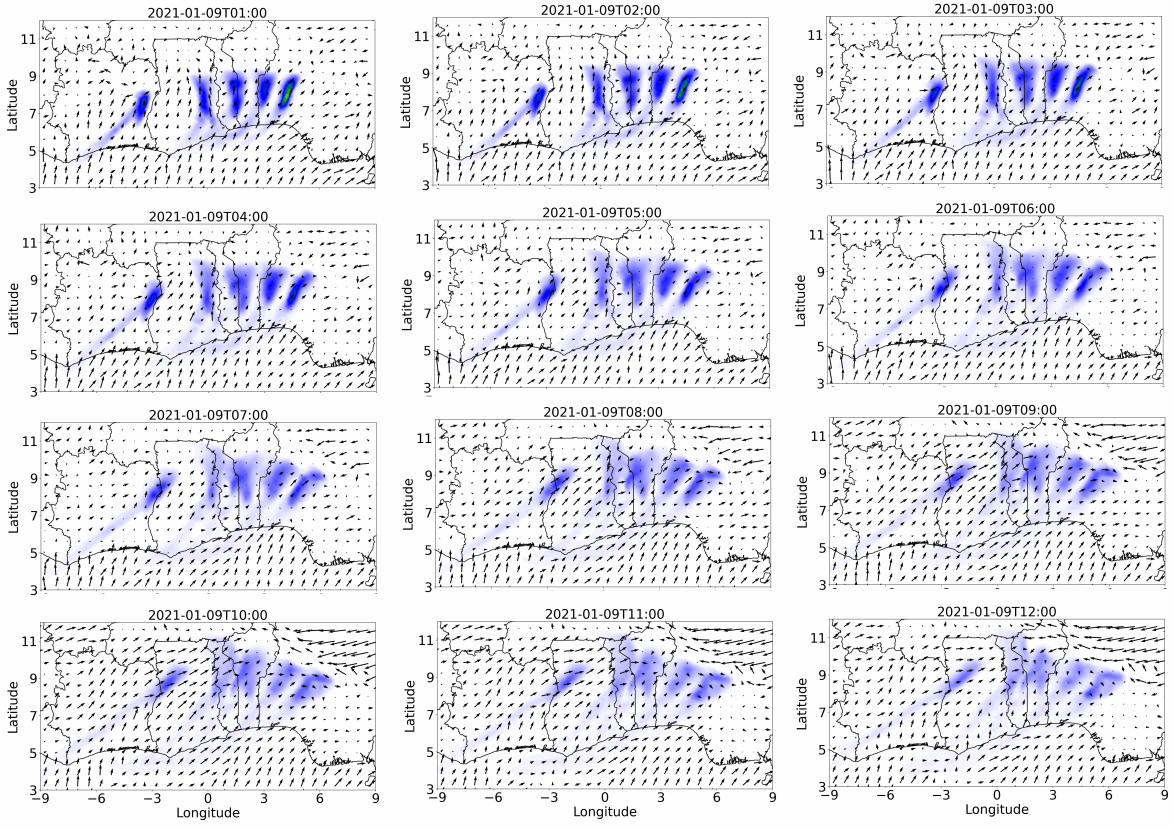

https://doi.org/10.5194/egusphere-2026-3128
Preprint. Discussion started: 23 June 2026

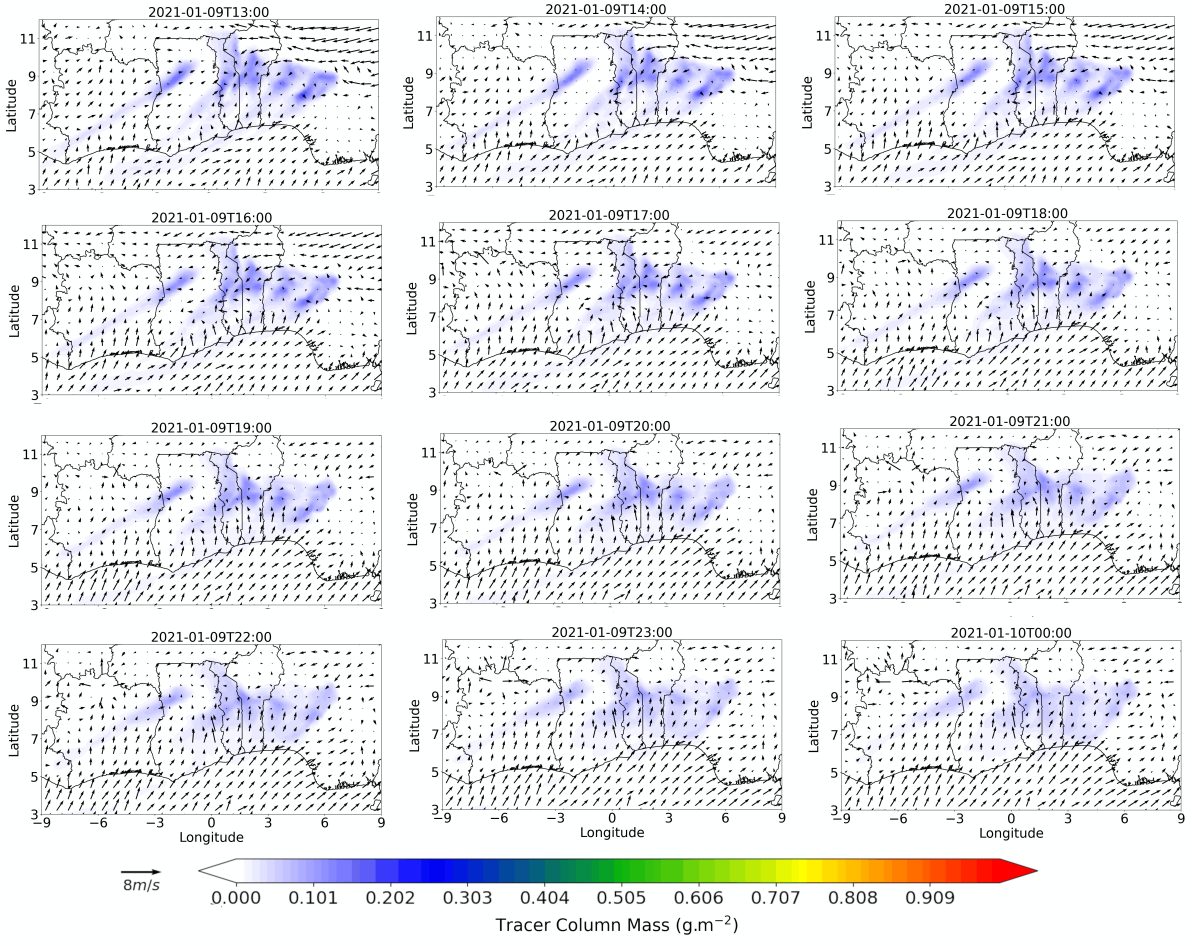

Figure A9. Hourly total pollutant column mass and 10m wind arrows dispersion. Pollutants are emitted from point sources in the main coastal cities (Abidjan, Accra, Lomé, Cotonou and Lagos) on 08 and 09 January 2021.